A doublecortin-domain protein of *Toxoplasma* and its orthologues bind to and modify the structure and organization of tubulin polymers

Jacqueline M. Leung[1*], Eiji Nagayasu[2*], Yu-Chen Hwang[3], Phillip G. Pierce[4], Isabelle Q. Phan[5], Robin Stacy[5], John M. Murray[1], Ke Hu[1]

[1]Department of Biology, Indiana University, Bloomington, IN, 47405, USA
[2]Department of Infectious Diseases, Division of Parasitology, Faculty of Medicine, University of Miyazaki, Miyazaki, Japan
[3]Nikon Instruments Inc., Melville, New York, 11747, USA
[4]UCB, and Seattle Structural Genomics Center for Infectious Disease, Bainbridge Island, WA, 98110
[5]Center for Global Infectious Disease Research, Seattle Children's Research Institute, and Seattle Structural Genomics Center for Infectious Disease, Seattle, WA, 98109, U.S.A

*: Equal contribution

Running title: Toxoplasma doublecortin-domain protein and orthologues

corresponding author:

kehu@indiana.edu

ABSTRACT

TgDCX is a doublecortin-domain protein that binds to the conoid fibers, a set of strongly curved tubulin-based non-tubular polymers in *Toxoplasma gondii.* Deletion of TgDCX impairs conoid structure and parasite invasion. TgDCX contains two tubulin-binding domains: P25-alpha and the DCX (doublecortin) domain. Orthologues are found in all Apicomplexans, their free-living marine relatives *Chromera* and *Vitrella*, and an early branching metazoan, *Trichoplax*. Here we report that isolated TgDCX-containing conoid fibers retain their pronounced curvature, but loss of TgDCX destabilizes the fibers. We crystallized and determined the 3D structure of the DCX domain of TgDCX, which is highly similar to those of human doublecortin. Doublecortin's ubiquitin-like folds are maintained and surface residues at the predicted tubulin contact sites are similar, and well-conserved among TgDCX orthologues. However, the orthologues vary widely in targeting to the conoid in *Toxoplasma* and in modulating the organization of microtubule arrays in *Xenopus* S3 cells. Several orthologues bind to microtubules in *Xenopus* cells, but only TgDCX generates short, strongly curved microtubule arcs. EM analysis shows microtubules decorated with TgDCX bundled into rafts, often bordered on one edge by a "C"-shaped incomplete tube. A *Chromera* orthologue closely mimics TgDCX targeting in *Toxoplasma* and binds to microtubules in *Xenopus,* but does not generate arced bundles or "C"-shaped incomplete tubes, and fails to rescue the defects of the TgDCX knockout parasite. These observations indicate that species-specific features of TgDCX are important for its function, and likely related to its unique ability to generate the strongly curved tubulin polymers in the cytoskeletal structure critical for efficient host-cell invasion.

INTRODUCTION

Microtubules are polymers, ubiquitous among eukaryotic cells, formed of tubulin subunits, which are extraordinarily well-conserved. The vast majority of microtubules in the eukaryotic systems examined to date are formed of 13 protofilaments. However, there are a number of exceptions. Microtubules with atypical numbers of protofilaments have been found in several organisms (for reviews, see (Chaaban and Brouhard, 2017; Davis and Gull, 1983; Dustin, 1984)). The B-tube in the doublet microtubule in the flagellum is an incomplete tube coupled with the 13-protofilament A-tube (Haimo and Rosenbaum, 1981). In the unicellular human parasite *Toxoplasma gondii*, a tubulin polymer that deviates significantly from the tube-form is found in the conoid (Hu et al., 2002). The conoid is a cytoskeletal complex of 14 fibers formed into a truncated cone. Each conoid fiber is a strongly curved [Figure 1A, (Hu et al., 2002)] folded ribbon formed of 8-9 tubulin protofilaments and follows a trajectory of a left-handed spiral. The unusual structure of the conoid fibers is not dictated by tubulin itself, because the tubulin subunits in these fibers are identical in amino acid sequence to those forming canonical microtubules elsewhere in the parasite (*e.g.* the cortical microtubules, intra-conoid microtubules, and microtubules in the mitotic spindle).

To search for the non-tubulin components responsible for the formation and maintenance of the unusual structure of the conoid fibers, a conoid-enriched fraction of the *Toxoplasma* cytoskeleton was analyzed by mass spectrometry, which revealed many novel candidate components (Hu et al., 2006). One of the proteins identified was TgDCX, localized exclusively along the conoid fibers (Nagayasu et al., 2016). TgDCX contains a doublecortin (DCX) domain and a partial P25α domain, two predicted tubulin-binding domains normally found separately in the proteins of mammalian neuronal cells. Human doublecortin, which contains two DCX domains, cooperatively binds to the groove between protofilaments (Bechstedt and Brouhard, 2012; Fourniol et al., 2010; Moores et al., 2004). P25α (also known as tubulin polymerization perturbing protein, TPPP) also binds to tubulin and modifies the structure of microtubules (Hlavanda et al., 2002). Mutations in the human *doublecortin* gene lead to gross disturbances in the architecture of the cerebral cortex: the double cortex syndrome in females and lissencephaly in males, due to perturbed neuronal migration during development. The partial P25α domain of TgDCX has in fact significant homology to typical DCX domains, so it is reasonable to

hypothesize that the P25α and DCX domains of TgDCX function in much the same way as the two DCX domains of doublecortin. The linker region between the partial P25α and DCX domains of TgDCX (44 aa residues) is slightly longer than that between the two DCX domains of doublecortin (35 residues).

Human doublecortin has been proposed to stabilize the13-protofilament microtubule structure in preference to other architectures that readily form when tubulin is polymerized in the absence of other proteins (Moores et al., 2004). This may be due to its ability to sense curvature in the protofilaments. It is intriguing that it seems to prefer strongly curved regions of microtubules in the presence of paclitaxel, and straight microtubules in the absence of paclitaxel (Bechstedt and Brouhard, 2012; Ettinger et al., 2016). Given this dramatic curvature-sensitive interaction of DCX domains with tubulin, TgDCX is clearly a prime candidate for the role of shaping conventional tubulin into unconventional highly-curved conoid fibers.

Although both the P25α and DCX domains are ubiquitous among metazoa, the presence of both domains in the same molecule appears to be almost exclusively an apicomplexan feature (Orosz, 2009; Orosz, 2016). This combination is found in all sequenced genomes of Apicomplexans (*e.g. Toxoplasma gondii, Plasmodium* spp. and *Cryptosporidium* spp.), as well as their photosynthetic (*Chromera velia* and *Vitrella brassicaformis*) and parasitic (*e.g. Perkinsus* spp.) relatives in the superphylum Alveolata. Beyond Apicomplexans and their relatives, the P25α+DCX arrangement is found in *Trichoplax adhaerens* from the phylum *Placozoa*, a primitive metazoan. Genomic sequence data from Eumetazoa occasionally appear with purported "apicortins", but these likely result from contamination with the DNA of an apicomplexan parasite infecting the Eumetazoan host (Orosz, 2018). An “apicortin” was also reported in the genome of the sperm whale (*Physeter macrocephalus)*, but this was likely due to infection of the whale by *Sarcocystis*, a common Apicomplexan parasite of marine mammals.

Previously we reported that TgDCX is specifically localized to the conoid in *Toxoplasma*, and that without TgDCX, the conoid structure becomes short and disordered, invasion of host cells is severely compromised, and the parasite forms many fewer and much smaller plaques relative to wild-type *Toxoplasma* (Nagayasu et al., 2016). We report here a

more in-depth analysis of the conoid fiber architecture, and a comparison of TgDCX and its eight orthologues from *Plasmodium falciparum* (an obligate intracellular parasite), *C. velia* and *V. brassicaformis* (free-living phototrophs), and *T. adhaerens* (an early diverging metazoan), utilizing localization *in vivo*, structural modeling based on the crystal structure of the DCX domain of TgDCX , and cross-complementation analyses in *Toxoplasma*. These comparisons revealed that neither microtubule binding nor conoid-targeting is sufficient for functional complementation. TgDCX alone has the unique ability of generating short, curved, and stable tubulin-containing polymers with a consistent curvature. This suggests that the divergent regions of TgDCX are important for modulating its function, and likely related to its ability to generate and stabilize tightly curved tubulin polymers.

RESULTS

TgDCX is specifically localized to the conoid in Toxoplasma and likely stabilizes the conoid fibers.

Proteins containing either the P25α or DCX domain are typically involved in interactions with microtubules (Bechstedt and Brouhard, 2012; Fourniol et al., 2010; Gleeson et al., 1999; Hlavanda et al., 2002; Moores et al., 2004). However, in *Toxoplasma*, TgDCX is specifically localized to the conoid fibers and is not associated with the canonical 13 protofilament (pf) microtubules that are present elsewhere in the same cell. Figure 1B-D shows the localization of TgDCX in parasites whose single endogenous genomic copy of *TgDCX* has been replaced with *mCherryFP-TgDCX* (*i.e.*, "mCherryFP-TgDCX knock-in" parasites). Colocalization with mNeonGreenFP-β1-tubulin shows that, in both interphase and dividing parasites (in which the daughters form inside the mother), mCherryFP-TgDCX is specifically concentrated in the conoids, but absent from all other tubulin-containing structures, such as the cortical microtubules or the centrosome. This localization is consistent with the conoid-specific structural defect when the *TgDCX* gene is deleted (Nagayasu et al., 2016) (Figure 1E-G).

To further characterize its structural role, we attempted to separate the TgDCX-containing conoid fibers from the rest of the cytoskeleton in wild-type (RH*Δku80Δhx*), *mCherryFP-TgDCX* knock-in, and *TgDCX* knockout parasites. Preparations from the wild-type and knock-in parasites contain intact conoids (Figure 2A-C) as well as numerous free conoid

fibers that are no longer associated with other structures in the apical complex. The conoid fibers are always curved into short arcs. In the intact conoid, the fibers follow inclined paths on the surface of a cone. The intersection of a cone with an inclined plane is an egg-shaped curve; *i.e.*, a closed curve with only one symmetry axis and continuously changing radius of curvature. However, for a cone with the dimensions of the retracted conoid and for a plane inclined at the angle of the conoid fibers, the intersection is nearly elliptical, with major and minor axes of the ellipse that differ by ~10%. The conoid fiber path covers much less than half of the circumference of the conoid, so in practice its shape can be closely approximated by an arc of a circle. The free conoid fibers all have similar arc length (355 ± 3.8 nm; sem, n=100), span the same arc angle (81.5 ± 1.2°), and have the same radius of curvature (253 ± 3.7 nm), indicating that these fibers are stable and their pronounced curvature is an intrinsic feature of their structure. In contrast, the fragments of cortical microtubules seen in the same image are all remarkably straight. Note that it is not possible to bend a microtubule into an arc as tight as that of the conoid fibers: when forcefully bent, normal microtubules snap before reaching curvatures this pronounced (Amos and Amos, 1991).

Close examination of the conoid fiber images commonly reveals a significant broadening of the fibers at their basal ends (i.e. the end closest to the apical polar ring when the conoid is extended) compared to the apical ends (i.e. the end closest to the preconoidal rings; *cf.* Figure 1), accompanied by more evident protofilaments. As the fibers have an asymmetric cross-section, similar to a dot-less elongated question mark ("?") or an inverted "J", their apparent width depends on the direction of view. Thus, the broadening at the basal end of the fibers is probably indicative of an inherent twist in the fiber, effectively changing the direction of view as one proceeds from apical to basal end (see the diagram in Figure 2). For reasons to be described later, we propose that this is a left-handed twist (see *Discussion*).

Although disordered conoid fibers can be observed in some intact conoids isolated from *TgDCX* knockout parasites (Figure 2D), free conoid fibers are not seen, suggesting that the conoid fibers are less stable without TgDCX. Alternatively, it is also possible that the fibers are more difficult to separate from the rest of the conoid in the absence of TgDCX. However, the

latter seems less likely, as one would have expected on occasion to encounter an isolated escaped fiber, or at least a fragmented conoid with fibers hanging loose, but these have never been seen.

TgDCX promotes the generation and stabilization of curved microtubules in a heterologous system

To characterize the effect of TgDCX on the structure of tubulin polymers in the absence of any other *Toxoplasma* proteins, ideally one would begin with *in vitro* reconstitution experiments using purified tubulin and TgDCX. Unfortunately this is not possible, as TgDCX protein *in vitro* is insoluble in buffers that are compatible with polymerization of tubulin (see *Methods*). As an alternate strategy, we characterized the interaction of these two proteins *in vivo* by expressing FP-tagged TgDCX in *Xenopus* S3 cells, which have neither conoid nor apical complex and do not contain apicomplexan-specific proteins. In this heterologous system, TgDCX coats tubulin-containing polymers and makes smoothly curved fibers (Figure 3). To determine the stoichiometry of TgDCX: tubulin dimer in this context, we measured the TgDCX content on these polymers using FP-TgDCX fluorescence and fluorescently-tagged *Sindbis* virus as the standard (Murray, 2017), which showed that the number of TgDCX molecules per unit of fiber length varied from ~0.25 molecules per 8 nm (the axial length of a single tubulin dimer) for the dimmest fibers (presumptive single microtubules) to ~2.0 per 8 nm for the brighter fibers, presumed to be bundles of several microtubules. The dimmer polymers (Figure 3B), which have lower TgDCX content per unit length, appeared to be more flexible (*i.e.,* meandered through the cytoplasm on idiosyncratic trajectories with mostly gentle curves, as do normal microtubules) than fibers with higher TgDCX content. Many of the TgDCX-coated fibers are bent into arcs with a similar radius of curvature, and are resistant to depolymerization by nocodazole treatment (Figure 3). Note that these arcs are much larger and much less sharply curved (radius of curvature 4.4 ± 0.1 µm; n=94) than the conoid fibers. Together, these results indicate that TgDCX can influence the organization, curvature, and stability of the polymers.

To determine which regions of the TgDCX molecule are critical for microtubule binding, bundling, and bending, we expressed mCherryFP-tagged truncations of TgDCX that included the DCX domain only (aa148-243) or both the P25α and the DCX domains (aa71-243) in *Xenopus* S3 cells. We found that mCherryFP-TgDCX148-243 does not localize to the microtubules,

indicating that the DCX domain alone is not sufficient for stable microtubule association (Figure 4A). This agrees with the published data on human doublecortin binding to microtubules, where both DCX domains are required (Taylor et al., 2000). On the other hand, mCherryFP-TgDCX71-243 binds to and generates curved microtubule bundles similar to those observed with the full-length protein, although with somewhat higher unbound cytoplasmic and nuclear fractions (Figure 4B). Thus, the N-terminal 70aa of the protein preceding the P25α domain contribute to binding efficiency, but are not required for microtubule binding, bundling, and bending. The difference in the ability of mCherryFP tagged TgDCX148-243 and TgDCX71-243 to bind to microtubules in *Xenopus* S3 cells is mirrored in conoid targeting in *Toxoplasma* (Figure 4C&D). When expressed in *Toxoplasma* (whether in the wild-type or in the TgDCX knockout background), mCherryFP-TgDCX148-243 was not enriched in the conoid. [Interestingly, a slightly longer fragment, eGFP-TgDCX135-256 also has a large cytoplasmic pool, but does bind very weakly to the adult conoid and is significantly enriched on daughter conoids and cortical microtubules (*data not shown*)]. The fragment that contains both the P25α and DCX domains, mCherryFP-TgDCX71-243, shows considerably more prominent binding to the conoids of both mother and daughter parasites with a lower concentration in the cytoplasm. Furthermore, expression of mCherryFP-TgDCX71-243 in the *TgDCX* knockout parasite largely reverses the dramatic structural and lytic cycle defects caused by a lack of TgDCX (Figure 4E-I). In contrast, we were unable to obtain a transgenic line stably expressing mCherryFP-TgDCX148-243, indicating that transfection of *TgDCX* knockout parasites with this truncated form does not confer a growth advantage, possibly because conoid targeting is required for the function of TgDCX.

Comparison of the structure, microtubule association, conoid targeting, and functional complementation between TgDCX and its orthologues

Organisms that contain TgDCX orthologues in their genomes differ greatly in lifestyles (*e.g.* obligate intracellular parasites *vs.* free-living phototrophs) and in conoid structures [*e.g.* a truncated cone made of non-tubular polymers in *Toxoplasma vs.* a sheet of canonical microtubules curved into an open-sided incomplete cone in *Chromera*, (Portman et al., 2014)]. Some of these organisms, such as *Trichoplax,* are thought to have no conoid-like structure.

The sequence conservation among the TgDCX orthologues is mostly restricted to the predicted P25-alpha and doublecortin domains (Figure 5A, Table 1) (Orosz, 2009; Orosz, 2016). Both the full-length TgDCX and the TgDCX71-243 fragment are insoluble in non-denaturing buffer systems (see *Methods*), but we were able to crystallize a fragment (AA148-243) that contains the DCX domain (Figure 5 and Table 2) and determine its structure by X-ray crystallography. The fold of TgDCX148-243 is very similar to that of the N-terminal DCX domain of human doublecortin (Figure 5B), which itself is quite similar (root mean square distance (rmsd) of ~ 2Å) to the doublecortin C-terminal DCX domain. [HsDCX-N and HsDCX-C, (Burger et al., 2016; Rufer et al., 2018)]. Comparing the three structures over the region in which they all align gives: TgDCX (6B4A, chain A, aa150-222) *vs.* HsDCX-N (5IOI, chain E, residues 51-128, rmsd 1.905 Å); TgDCX (6B4A, chain A, aa150-222) *vs.* HsDCX-C (5IP4, chain E, residues 178-252, rmsd 1.99 Å). Residues responsible for the four tubulin contact regions between HsDCX-N and tubulin identified by structural docking (Fourniol et al., 2010) are in most cases similar.

Given the high level of homology among the TgDCX orthologues in the region of their DCX domains (Figure 5A, Table 1), we used the structure of TgDCX148-243 as a model for threading (Figure 5C&D) the corresponding regions in the TgDCX orthologues in *Chromera velia* (CvDCX1, CvDCX2, CvDCX3), *Vitrella brassicaformis* (VbDCX1, VbDCX2, VbDCX3), *Plasmodium falciparum* (PfDCX), and *Trichoplax adhaerens* (TaDCX). This comparison revealed a clear difference between the apicortins that do and do not bind strongly to microtubules in *Xenopus* (Figure 6, Table1, see below for detailed description). At the location reported in (Fourniol et al., 2010) corresponding to tubulin contact region #3 in HsDCX-N (K53), which abuts a strongly electronegative patch on β-tubulin, orthologues that bind to microtubules have a positive charge (R152 in TgDCX, lysine in VbDCX1, CvDCX1, and PfDCX), whereas the orthologues that do not bind have isoleucine. Unfortunately, a simple electrostatic mechanism for binding enhancement is complicated by the orientation of this residue: in both the TgDCX and HsDCX-N 3D structures, this positively-charged sidechain is oriented away from tubulin, not towards it. Thus the significance of the correlation between amino acid identity at this position and microtubule binding is not yet clear. The comparison of orthologues also revealed a reversal of polarity at one position: D201 in TgDCX and D at the

corresponding location in CvDCX1, VbDCX1 and PfDCX, is replaced by K or R at the corresponding residue in CvDCX2, CvDCX3, VbDCX2, VbDCX3, and TaDCX. Thus this polarity reversal also correlates with microtubule binding, but as this location is also on the surface facing away from the microtubule, then if the correlation is more than just coincidence, the explanation for this effect on microtubule binding is also presently unclear.

To examine the extent of conservation in microtubule and conoid association among these orthologues, we expressed mCherryFP tagged orthologues of TgDCX in *Xenopus* S3 cells (Figure 6) and in *Toxoplasma* (Figure 7). No significant microtubule localization was found for mCherryFP tagged CvDCX2, CvDCX3, VbDCX2, and VbDCX3 in *Xenopus* cells (Figure 6, Table 1). In contrast, CvDCX1, VbDCX1, and PfDCX are prominently localized to the microtubules. However, none of them generates the short and arced microtubule bundles observed when FP- tagged TgDCX is expressed in *Xenopus*. Some mCherryFP-TaDCX associates with microtubules but the unbound cytoplasmic fraction is large, much larger relative to the bound fraction than is the case for the three orthologues that do bind strongly.

In *Toxoplasma*, we expressed FP-tagged orthologues under the control of the α-tubulin promoter (Figure 7). We have previously shown that TgDCX-eGFP expressed from an α-tubulin promoter can complement the structural, invasion and lytic cycle defects of the *TgDCX* knockout parasite [(Nagayasu et al., 2016), also see Figure 4]. When transiently expressed from this promoter, TgDCX-eGFP is targeted to the conoid efficiently (Figure 7A-B). However, in contrast to the exclusively conoidal localization observed with TgDCX, mCherryFP-TgDCX, and TgDCX-mNeonGreenFP when driven by the endogenous TgDCX promoter (Figure 1B-D) (Nagayasu et al., 2016), expression of FP-tagged TgDCX driven by the α-tubulin-promoter sometimes results in decoration of the daughter cortical microtubules, centrosomes and basal complex. This reveals that the specificity of conoid association by the TgDCX protein is not absolute, and likely modulated by regulation at the transcription and post-translational level. Notably, while FP-tagged TgDCX can coat the daughter cortical microtubules when expressed from the α-tubulin promoter [which is essentially constitutive, (Behnke et al., 2010), Figure7D], it does not stay bound to the cortical microtubules of the adult parasite, revealing a change in the surface property of the cortical microtubules as the parasite becomes mature.

The conoid targeting efficiency of the TgDCX orthologues varies widely (Figure 7C, Table 1). TaDCX is not enriched in the conoid. CvDCX2, CvDCX3, VbDCX2, VbDCX3, and PfDCX are prominently associated with the daughter conoid, but barely detectable in the mother conoid. This reveals that while conserved features in these orthologues allow them to interact with components of an assembling conoid, the structural tolerance for the divergent features decreases as the conoid matures. VbDCX1 is targeted to both mother and daughter conoids but also shows prominent unbound cytoplasmic, mitochondrial and nuclear pools. CvDCX1, which shares the highest sequence similarity with TgDCX (44% identical, 57% similar over the full-length), largely mimics the localization of TgDCX when its expression is driven by the α-tubulin promoter. It is prominently localized to the conoids of both adult and daughter parasites, and sometimes to the cortical microtubules and centrosomes of daughter parasites, with only a small cytoplasmic pool.

Despite the similar localization pattern between CvDCX1 and TgDCX, when CvDCX1 is expressed in the *TgDCX* knockout background, it fails to complement the defects in conoid structure and in the lytic cycle (Figure 8). EM examination of negatively-stained whole-mount parasites showed that *ΔTgDCX* parasites expressing CvDCX1 still have a distorted conoid structure like the knockout parasites. Contrast this with the restored conoid structure in *ΔTgDCX* parasites expressing full-length TgDCX or TgDCX71-243 (Figure 4G and H).

To further determine how TgDCX and CvDCX1 differentially modify the organization and structure of tubulin polymers, we carried out correlative light and electron microscopy analysis of *Xenopus* S3 cells expressing FP-tagged TgDCX, TgDCX71-243, and CvDCX1 (Figure 9 & 10). In untransfected (Figure 9A and B) and FP-CvDCX1 transfected (Figure 9C-E) *Xenopus* S3 cells, microtubules invariably have 13 protofilaments (pf) and are closed tubes. In contrast, TgDCX (Figure 10A) or TgDCX71-243 (Figure 10B) containing fibers are mostly single-layered, occasionally multi-layered, rafts of microtubules, each layer containing 2-10 microtubules arranged side by side in a plane. The planar raft-like arrangement is most simply understood as the natural consequence of "zipping" curved microtubules together: the distance over which neighboring microtubules remain in contact is greatly increased if the microtubules

are stacked side-by-side, all bending in the same direction. Notably, ~40% of the rafts are bordered on one edge by an incomplete tube. This "C"-shaped element appears to be a 13-protofilament microtubule with an opening on one side, the side that faces the edge of the sheet. The "C"-shaped incomplete tubes are also seen as single fibers, not associated with a raft. Among all the microtubules with clear profiles in three different cells, 36% were "C"-shaped incomplete tubes (114 out of 313). The diameters of TgDCX or TgDCX71-243 containing tubes are often greater than the canonical 13-pf microtubules. Some of the microtubules contain more than 14 protofilaments (Figure 10C).

Thus, while the sequence conservation between CvDCX1 and TgDCX is high and sufficient for similarly specific localization to the conoid, enough variations have accumulated during the evolutionary divergence of these two lineages to result in a difference in their abilities to restore the conoid structure of the *TgDCX* knockout parasite and support the parasite lytic cycle. This is likely related to a difference in their impact on the arrangement of the protofilaments, and on the organization and curvature of the tubulin polymers.

DISCUSSION

The conoid originated early in the evolutionary history of the apicomplexan parasites. It is present in all coccidians examined to date (*e.g. Toxoplasma* and *Eimeria* spp.). Although Apicomplexans in *Haemosporidia* (*e.g. Plasmodium* spp.) are classified as *Aconoidasida* ("conoidless"), a conoid-like structure was found in the ookinete stage of *Plasmodium* and other haemosporidians by EM (Desser et al., 1970; Patra and Vinetz, 2012). The level of *PfDCX* transcription relative to the whole transcriptome is much higher in the gametocyte and ookinete stages compared with those in the blood stages. Furthermore, even though it has a divergent P25α domain, PfDCX binds strongly to microtubules when expressed in *Xenopus* S3 cells and to daughter conoids when expressed in *Toxoplasma.* It is therefore a useful probe to determine whether *Plasmodium* spp assemble a conoid-like structure at certain stages of their life-cycle, and the organization of the protofilaments in the "conoid" fibers if such structure exists.

It is interesting to consider the geometry of the arrangement of conoid fibers in the conoid, particularly with respect to the changes that must occur upon conoid extension. As part of the *T. gondii* lytic cycle, which is the fundamental pathogenetic event in toxoplasmosis, in response to the signal of elevated intracellular [Ca^{2+}], the parasite activates motility to exit its lysed host cell and extends the conoid. Extension is accompanied by a change in the shape of the conoid as it becomes less conical and more cylindrical, while the pitch of the conoid fibers becomes steeper (Hu et al., 2002). In the retracted state, the conoid is a truncated cone, widening from a diameter of ~400 nm at the top to ~600 nm at its basal end, with conoid fibers angled at ~25° relative to base of the conoid. For this geometry, the conoid fibers follow a path with radius of curvature varying from 250 to 260 nm, close to what is observed for isolated fibers in the cryoEM images. After extension, the apical diameter is unchanged, but the basal diameter has decreased to ~450nm, the conoid has become taller and more cylindrical, and the angle of the conoid fibers has increased to ~40°. The fibers follow a more steeply inclined, and therefore less curved path: the radius of curvature for the fiber path in the extended conoid has a radius of curvature varying from ~300 to ~340 nm, somewhat larger than observed for isolated fibers. From these admittedly approximate calculations, we propose that when released from the conoid, the fibers adopt the configuration characteristic of the retracted state, and that this therefore is the lower energy, most strain-free, configuration.

The change in pitch during conoid extension results in the fibers becoming more parallel to the conoid central axis. This necessitates a change in twist of the fiber (unless both ends are free to rotate, which seems less plausible). The change in pitch can be accomplished by a rotation around the central axis of the base of the conoid relative to its apex, clockwise viewed from the apical end. The consequence for the fibers is twisting in a right-handed manner. However, EM images of cross-sections of the extended conoid (Hu et al., 2002) show that the fibers have little or no twist along their length (see the model in Figure 11), suggesting that in the retracted-conoid state, the fibers are twisted in a left-hand manner and then untwist as a consequence of conoid extension. This again suggests that the fibers seen in the cryoEM images are in the configuration (*i.e.*, twisted) they have in the retracted conoid.

The apicomplexan parasites are thought to have evolved from a free-living marine protozoan with conserved ancestral traits and cellular features. Indeed, a "pseudoconoid" is present in the marine relatives of the Apicomplexans, such as *C. velia* and *V. brassicaformis.* In *Chromera*, the pseudoconoid is a half-cone formed from a sheet of 30-35 canonical microtubules (Portman et al., 2014), in which the curvature of the microtubules is considerably weaker than that of the conoid fibers in *Toxoplasma.* Thus, the conoid underwent considerable structural rearrangements during the evolution of the intracellular parasitic lifestyle of the Apicomplexans. Characterization of the components of the conoid might help to understand the molecular basis of these lifestyle transitions. If we presume that the pseudoconoid as seen in *Chromera* is similar to the ancestral form of the conoid in *Toxoplasma,* then the ancestral form of TgDCX very likely binds to microtubules, which form the pseudoconoid. Our observation that TgDCX can associate with microtubules in *Xenopus* S3 cells is consistent with this hypothesis. However, as TgDCX binds quite readily to canonical microtubules, it is puzzling that it can be specifically localized to the conoid in *Toxoplasma* in the presence of several other tubulin-containing structures (Figure 1, *mCherryFP-TgDCX* knock-in parasite), particularly since the same tubulin subunits are assembled into the non-tubular conoid fibers simultaneously and in close proximity to forming canonical (tubular) microtubules during daughter construction (Nagayasu et al., 2016). When expressed from a strong constitutive promoter, FP-tagged TgDCX is predominantly localized to the conoid, suggesting preferential binding to non-tubular tubulin polymers (Figure 7). However, expressed in this manner, TgDCX also binds to daughter cortical microtubules, indicating that the specific conoid targeting in *Toxoplasma* must involve other levels of control, such as transcriptional regulation in combination with post-translational modifications of TgDCX and its targets.

Similar to TgDCX, one orthologue each from *Chromera* and *Vitrella* (CvDCX1 and VbDCX1) were observed to associate with microtubules in *Xenopus* S3 cells and are targeted to the conoid in *Toxoplasma*. However, given the strong sequence conservation of the TgDCX orthologues in the P25α and DCX domains, including the residues predicted to serve as tubulin contacts, it is surprising that the efficiency of microtubule and conoid association vary so widely. For instance, all three orthologues in *Chromera* share a high degree of conservation with TgDCX, but CvDCX2 and CvDCX3 show no significant enrichment on the microtubules in

Xenopus S3 cells and are not efficiently targeted to the conoid of mature parasites when expressed in *Toxoplasma.* While we predict that CvDCX1 is localized to the pseudoconoid in its native environment, it will be of interest to characterize all three orthologues in *Chromera* and determine whether they have overlapping or distinct localization and functions.

During the divergence of the Apicomplexans, the precursor gene for *TgDCX* must have accumulated *Toxoplasma*-specific features for maintaining the structural integrity of the conoid and facilitating invasion, as the expression of the orthologue (CvDCX1) that most closely mimics the localization of TgDCX in *Toxoplasma* fails to restore the conoid structure and also fails to complement the lytic defects of *TgDCX* knockout parasite. One such specific feature might be TgDCX's ability to generate and stabilize curved tubulin polymers (Figures 3-4), which might contribute to the stabilization of the highly curved conoid fibers of *Toxoplasma.* However, we note that TgDCX is unlikely to be the only factor that contributes to the bending of the conoid fibers, because: 1) distorted fibers can sometimes be observed in the conoid of the TgDCX knockout parasite (Figure 2); 2), the radius of curvature of the arced microtubules seen in the *Xenopus* cells is significantly greater than that of the conoid fibers (4.4 *vs*. 0.25 μm); and 3), the incomplete tubes formed in *Xenopus* cells in the presence of TgDCX are more similar to microtubules than to the conoid fibers (in cross-section, incomplete circles rather than inverted "J" shapes). Interaction with microtubules differs dramatically between TgDCX and its orthologues, also between TgDCX and human doublecortin. Ultimately these differences must arise from differences in the 3D structure of TgDCX compared to the other proteins. The quality of the structural data for the DCX domains of both TgDCX and doublecortin is certainly high enough to identify differences in their 3D structure at the required level of detail, and that is essential for further progress, but unfortunately that is only a part of the requirement. The significance of small differences in structure of the DCX domains will be apparent only when high-quality 3D structures of both the undecorated microtubule and the full-length TgDCX-(or doublecortin-) decorated microtubule become available. It is worth pointing out that presently this is far from the case. At the ~8Å resolution of the currently available structure for the complex between microtubule and a single doublecortin domain (Fourniol et al., 2010) there is considerable uncertainty as to the exact orientation of the bound DCX domain, and indeed, some uncertainty as to whether it is HsDCX-N or HsDCX-C that is present in the map. Therefore it is

not possible at present to convert structural details into an understanding of how TgDCX bends microtubules, and why its orthologues do not. A particular example of this general problem is the correlation we observed between microtubule binding and amino acid sequence at two locations, both of which, according to the published orientation of the DCX domain, would be facing away from the microtubule contact surface. Perhaps the published orientation is correct, and our correlation is in that case either coincidence or an indication of some allosteric effect. On the other hand, the published orientation may not be applicable for TgDCX and its orthologues.

By combining localization, structural and cross-complementation analyses, we discovered that TgDCX orthologues from organisms with drastically different lifestyles have distinct polymer binding and modifying capabilities. In the future, systematic comparison of orthologues of conoid components in the Apicomplexans and their marine relatives will be informative to determine if and how the molecular and structural changes in the conoid-like structures contribute to the transition from the free-living to the parasitic lifestyle of the Apicomplexans.

METHODS

Culture, harvest, and transfection of Toxoplasma gondii

T. gondii tachyzoites were used in all experiments, and grown in monolayers of human foreskin fibroblast (HFF) cells (Roos et al., 1994). Transfection of *T. gondii* tachyzoites was carried out as previously described (Heaslip et al., 2010) using 30-40 µg of plasmid DNA in "cytomix" buffer (120 mM KCl; 0.15 mM $CaCl_2$; 10 mM KH_2PO_4 / K_2HPO_4; 25 mM HEPES; 2 mM K_2EGTA; 5 mM $MgCl_2$, 2 mM K_2ATP, 5 mM glutathione; pH adjusted to 7.6 with KOH).

Plaque assay

Plaque assays were performed as previously described (Nagayasu et al., 2016).

Xenopus S3 cell culture, transfections, and nocodazole treatment

Xenopus S3 cells stably expressing eGFP-tubulin were maintained at room temperature (22ºC) in 70% Leibovitz's L-15 medium (ThermoFisher Scientific-Gibco, Cat#11415-064), 15% Fetal Bovine Serum, 15% H_2O, 1% Penicillin/Streptomycin (ThermoFisher Scientific-Gibco, Cat#15140-122), and 72 µM G418 (ThermoFisher Scientific, Cat#10131035). For transfection, Lipofectamine® LTX Reagent with PLUS® Reagent (ThermoFisher Scientific, Cat#15338100) was used with the conditions recommended by the manufacturer, and 2.5 µg of plasmid DNA. In some experiments, ~16 hours after transfection, cells were treated with 16.6 µM nocodazole (Sigma # M1404) for 30 min to 2 hours before imaging.

Plasmid construction (All PCR primers and synthesized gBlock gene fragments are listed in Table 3).

After construction, plasmids were used to transform chemically competent TOP10 cells by heat shock, or electrocompetent DH5α cells (New England Biolabs, Cat# C2989) by electroporation. Plasmid DNA was isolated by standard procedures and the constructions were verified by DNA sequencing.

For the ptub-based plasmids driving expression in *Toxoplasma* of *Chromera* and *Vitrella* orthologues CvDCX1-3 and VbDCX1-3, ptubg-[DCX orthologue]-mNeonGreenFP was generated with a three-component assembly using the NEBuilder HiFi Assembly kit (New

England Biolabs, E2621S) according to the manufacturer's instructions. The vector backbone was prepared by removing the 12-base pair stuffer sequence in ptubg (Nagayasu et al., 2016) using *Nhe*I and *Afl*II. The mNeonGreenFP coding sequence was amplified using primers S1 and AS1 with the plasmid pmNeonGreenFP-N1 as a template [(Shaner et al., 2004; Shaner et al., 2013); a kind gift from Richard Day]. The coding sequence for the DCX orthologue including the ATG initiation codon but lacking the stop codon, and flanked by the linker sequences 5'-gaattccctttagatccgctagcaaa-3' at the 5' end and 5'-cagatcctgttcctcc-3' at the 3' end, was synthesized as a gBlock gene fragment (Integrated DNA Technologies; Coralville, IA). Coding sequences for DCX orthologues of *Chromera velia* reference strain CCMP2878 and *Vitrella brassicaformis* reference strain CCMP3155 were obtained from CryptoDB (Heiges et al., 2006) (http://cryptodb.org/cryptodb/, release 41). Sequences for all gBlock gene fragments are listed in Table 3.

ptubg_PfDCX-mNeonGreenFP was generated with a four-component HiFi assembly as described above for the *Chromera* and *Vitrella* orthologues, except Exons 1 and 2 of PfDCX were amplified using primer pairs S2 and AS2, and S3 and AS3, respectively, using *P. falciparum* 3D7A genomic DNA (BEI Resources, Manassas, VA, Cat# MRA-151G, contributed by David Walliker) as the template.

ptubg_TaDCX-mNeonGreenFP was generated with a three-component HiFi assembly as described above for the *Chromera* and *Vitrella* orthologues, except the coding sequence of TaDCX was amplified using primers S4 and AS4 using ptub-mEmeraldFP-TaDCX (synthesized by GenScript Inc, NJ) as the template.

The coding sequences for TgDCX truncations (TgDCX148-243 and TgDCX73-243) were PCR amplified from pTKO4_mCherryFP_TgDCX (Nagayasu et al., 2016) with primer pairs S5-AS5 and S6-AS6 respectively, and cloned into ptubg, fused to the C-terminus of mCherryFP (PCR amplified with primers S7-AS7), in a three-component NEBuilder HiFi assembly as described above for the TgDCX orthologues.

These same TgDCX truncations were PCR amplified with primer pairs S8-AS8 and S9-AS9 respectively for cloning into an expression plasmid for *Xenopus* cells utilizing the CMV promoter. The CMV-promoter plasmid, pC22, was derived from Clontech vector pEGFP-C2 by cutting with *EcoR*I plus *Xma*I, and inserting the adaptor formed by hybridization of oligos S10 and AS10. Plasmid pC22_mCherryFP-HsTUBA1 was constructed from the *Nhe*I-*Afl*II fragment of pC22 by ligation of a PCR fragment containing mCherryFP-HsTUBA1, amplified with primers S11 and AS11 from plasmid pCMV_mCherryFP_HsTUBA1, a gift from the laboratory of Dr. Roger Tsien (Shaner et al., 2004). The human tubulin sequence in pC22_mCherryFP-HsTUBA1 was excised with *Bgl*II-*Afl*II and replaced with the PCR amplified TgDCX fragments via a two-component NEBuilder HiFi assembly reaction.

CMV-promoter expression plasmids for the TgDCX orthologues were similarly derived from pC22_mCherryFP-HsTUBA1 using PCR products amplified with primers S12-AS12 (Cvel_6797), S13-AS13 (Cvel_18664), S14-AS14 (Cvel_28653), S15-AS15 (Vbra_12284), S16-AS16 (Vbra_15441), S17-AS17 (Vbra_21191), and S18-AS18 (Pf3D7_0517800).

To construct the plasmid for expressing His-tagged recombinant TgDCX148-243 (BG1861_ TgDCX148-243), the coding sequence was amplified from the genomic DNA of *Toxoplasma gondii* strain ME49 and cloned into an *E. coli* expression vector (BG1861) using ligase-independent cloning (Aslanidis and de Jong, 1990). The expression construct includes a non-cleavable N-terminal His_6 tag. The coding sequence for the recombinant protein is deposited in the SSGCID database (ID: TogoA.17199.a.B3.GE41306).

Creating CvDCX1-mNeonGreenFP transgenic parasites in the TgDCX knockout background. The ptubg_CvDCX1-mNeonGreenFP plasmid was electroporated into *TgDCX* knockout parasites, which have been described previously (Nagayasu et al., 2016). The transfected population was subjected to five rounds of 20 μM chloramphenicol selection, and clones were individually screened for mNeonGreenFP fluorescence. The growth of the clones was compared with the *TgDCX* knockout, knock-in, and TgDCX complemented parasites using plaque assays.

Light Microscopy

Wide-field image stacks were acquired at 37°C using a DeltaVision imaging station (GE Healthcare / Applied Precision) fitted onto an Olympus IX-70 inverted microscope base as described in (Nagayasu et al., 2016). 3D-structured illumination (SIM) images were collected on a DeltaVision OMX Blaze system using a 100x NA 1.35 or 60X NA 1.42 objective with 3 orientations and 5 phases for the illumination pattern and a z-spacing of 0.125 µm. Image stacks were deconvolved with the manufacturer supplied software and locally measured wavelength-specific PSFs. *Contrast adjustment*: In the raw data, the range of reliably measured intensities often exceeds 200-fold. On a good monitor with linear mapping, perhaps a 30 fold range can be displayed. For print media, the range is even smaller. Therefore, with a linear mapping of data intensities to display media, it is not possible to display the biologically and statistically significant image data without making dim structures invisible or bright structures saturated. For this reason, we have routinely adjusted contrast levels with non-linear mapping (*i.e.,* gamma not equal to 1) to allow the reader to see both dim and bright features in cells of interest.

Electron microscopy of whole mount Toxoplasma

Electron microscopy of detergent-extracted whole mount *Toxoplasma* cytoskeleton was performed as previously described in (Nagayasu et al., 2016).

Electron microscopy of intact and disassembled conoids

Isolated conoids were prepared by first treating a suspension of ~ 10^8 extracellular parasites with 1 ml of a calcium-saline (138 mM NaCl, 2.7 mM KCl, 20 mM K^+HEPES pH 7.6, 5 mM $CaCl_2$) plus 25 µM A23187 to cause extension of the conoid (Mondragon and Frixione, 1996). After 5 min, the parasites were lysed by washing with 1 ml of detergent-containing buffers of decreasing ionic strength (first, 5 mM CHAPS [Sigma #C5070], 1 mM Tris acetate, pH 7.5, 10 mM K_2EGTA; second, the same except 5 mM K_2EGTA; third, two times with the same solution without K_2EGTA). After each wash, the parasites were collected by centrifugation at 4500 x g for 5 min. The lysed parasites were resuspended in 2 ml of the final wash buffer in a 15 ml plastic tube and sonicated on ice twice for 30 sec, with cooling for 1 minute between pulses. The suspension was centrifuged at 13,200 x *g* for 5 min and the supernatant was discarded. The barely visible pellet, which contained mostly isolated conoids plus intact or fragmented apical polar rings, was resuspended in 100 µl 20 mM K^+HEPES, pH 7.5. To prepare dissociated conoid

fibers, the conoid prep was treated with 10 μg/ml α-chymotrypsin at room temperature for 6 min. Digestion was stopped by addition of TPCK (Sigma # T4376) to 100 μM. For cryoEM, a few μl of suspension was placed on an EM grid coated with a lacey carbon film, blotted with filter paper, and immediately frozen by plunging into a rapidly-stirred liquid propane:isopentane mixture (~19:1, v/v) held at liquid nitrogen temperature. Frozen grids were searched in a Phillips 400 EM for appropriate areas at low illumination and defocus of ~0.8 mm. Low dose images were acquired at 28,000 magnification, at 120 kev, and defocus of 1.6 or 2.0 μm. For negative staining, the suspension was allowed to adsorb for 15 min to a carbon-coated EM grid, negatively stained with 2% phosphotungstic acid, and imaged in a JEOL 1010 at 80kev, or a JEOL1400 Plus at 120kev.

Correlative Light and Electron microscopy of Xenopus S3 cells transfected with a plasmid expressing fluorescently tagged TgDCX or CvDCX1.

3D stacks of LM images of suitable cells in a 35 mm glass-bottom dish were recorded as described above at 60x magnification. Lower magnification (20x, 10x, and 4x) images of the same area were then recorded to facilitate relocating the same cells after embedding for EM. The dish of cells was simultaneously partially fixed and permeabilized by replacing the culture medium with Buffer 1 (100 mM Na^+MES, 2 mM $MgCl_2$, 100 μM $CaCl_2$, 1 mM CaEGTA, pH 6.6) plus 100 mM glutaraldehyde and 0.5% Triton X-100. After shaking for 1 minute at room temperature, the cells were further permeabilized with 0.5% Triton X-100 in Buffer 1 for 30 min, then fixed with 100 mM glutaraldehyde plus 1% tannic acid (Sigma # T0125) in Buffer 1 for 2-4 hrs. After carefully aspirating off all of the fixative, 40 mM OsO_4 in 15 mM $NaHPO_4$ pH 6.0 was added and the dish was shaken at 4 ^oC for 1 hour. The dish was rinsed three times with H_2O, shaken with 1% uranyl acetate for 4 hr, then dehydrated for 5 min each with 50%, 70%, and 95% EtOH, then with 100% EtOH for 5 min twice. The sample was infiltrated with freshly prepared Spurr resin: acetone (1:3) for 1 hr, then 3:1 for 1 hour, and 100% Spurr resin for ~16 hr. The resin was aspirated off, replaced with 400 μl of fresh resin, covered with a glass coverslip, and polymerized at 66 ^oC for ~ 16 hr. Cells originally imaged by LM were relocated by bright-field microscopy at 10X magnification in this thin sheet, and their locations marked. The glass coverslips on both sides of the thin resin layer were dissolved using concentrated HF, preserving the marked locations, and the thin sheet of resin containing the monolayer of cells was cut into

small pieces, each piece containing one of the originally imaged cells. These small pieces were then placed in a block-mold, carefully oriented to allow sectioning perpendicular to the plane of the cell monolayer, and with optimal rotational orientation of the target cell. After re-embedding in a block of Spurr resin, the block was carefully trimmed so that the mesa for sectioning contained only the desired cell with a small margin on each side. Silver sections were cut with a diamond knife, deposited on bare or carbon-coated Cu grids, stained for 30 min with 6% uranyl acetate in 50% methanol, then for 5-10 min with Reynold's lead citrate, and examined in a JEOL1400 EM at 120kev.

Expression of recombinant TgDCX

TgDCX expressed in bacteria, tagged with hexahistidine or fused to maltose-binding protein, could be solubilized only in the presence of denaturing detergents, GuCl, or urea. Attempted removal of the denaturing agents and refolding by a variety of methods always resulted in precipitation of the TgDCX. The same is true of a TgDCX fragment containing the P25α and DCX domains (*i.e.*, lacking the first 70 aa). Expression of His_6-tagged TgDCX in yeast (*K. lactis*), or of HAT-tagged mNeonGreenFP-TgDCX in HEK293E cells driven by the CHEF1 promoter also gave no soluble protein under non-denaturing conditions. An initial small scale expression of His_6-mNeonGreenFP-TgDCX in Sf9 cells yielded some protein with microtubule binding and bundling activities, but the purity was poor. Subsequent larger scale purifications yielded no soluble full-length protein using physiological buffers for extraction. Abundant soluble recombinant protein could be obtained by extracting the Sf9 cell pellet with 0.3 M CHAPS or Zwittergent 3-10 plus 3 M GuCl or stronger denaturing buffers, but removal of the detergent/denaturant inevitably led to immediate irreversible precipitation of all the TgDCX.

Purification and Crystallization of recombinant His-tagged TgDCX148-243

His-tagged recombinant TgDCX148-243 (SSGCID ID: TogoA.17199.a.B3.PW38274) was expressed in *E. coli* Rosetta BL21 (DE3) transformed with the plasmid BG1861_ TgDCX148-243 following standard SSGCID protocols as described previously (Choi et al., 2011). Purification was completed using Ni-NTA affinity and size exclusion chromatography following standard SSGCID protocols (Bryan et al., 2011). The purified protein was concentrated to 15 mg/mL in its final buffer (25 mM HEPES pH 7.0, 500 mM NaCl, 5% glycerol, 2 mM DTT, and

0.025% sodium azide), flash frozen in liquid nitrogen, and stored at -80°C. All crystallization experiments were completed in 96-well XJR trays (Rigaku Reagents) with 0.4 µl protein and 0.4 µl reservoir solution as sitting drops equilibrated against 80 µL reservoir. Crystallization trays were incubated at 14°C. Diffraction quality crystals were obtained in PACT Premier HT-96 (Molecular Dimensions) condition E6 (18% w/v PEG3350, 200 mM sodium formate). Experimental phases were obtained by soaking these crystals in reservoir containing 20% of a 2.5 M sodium iodide solution in ethylene glycol as cryoprotectant before vitrification by dipping in liquid nitrogen. The phasing information from this crystal was then applied to data collected from a separate crystal obtained using an optimization screen based on PACT E6 (24.09% w/v PEG3350, 50 mM sodium formate), which was soaked in 20% ethylene glycol as cryoprotectant and vitrified by dipping in liquid nitrogen.

Data Collection and Structure Solution of recombinant TgDCX148-243

Data sets were collected in-house at 100 K on a Rigaku FR-E$^+$ SuperBright rotating anode equipped with Rigaku VariMax optics and a Saturn 944+ CCD detector, using CuKα X-rays. All data sets were reduced with the XDS (Kabsch, 2010) (Table 2). For the iodide data set, Friedel pairs were kept separate. Friedel pairs were merged for the data set used for refinement. For the iodide-soaked crystal, 11 anomalous sites were found with HySS (Grosse-Kunstleve and Adams, 2003) using data up to 2.00 Å resolution. The anomalous sites were further refined, and initial phases were calculated with Phaser_EP (Read and McCoy, 2011) within the CCP4 package (Collaborative Computational Project, 1994). The CCP4 program PARROT (Cowtan, 2010) was used for phase improvement; NCS averaging was not used due to low NCS correlations. An initial model was built with ARPwARP (Langer et al., 2008).

Structure Refinement and Validation of recombinant TgDCX148-243

Molecular Replacement using the experimentally-phased model was completed with Phaser (McCoy et al., 2007) within the Phenix ligand pipeline. All structures were refined in PHENIX (Adams et al., 2010). Manual model building was completed using Coot (Emsley et al., 2010). The quality of all structures was assessed using built-in tools in Coot and using Molprobity (Chen et al., 2010) through the Phenix interface. The coordinates and structure factors were deposited in the PDB under accession code (6B4A).

Structural modeling of TgDCX orthologues based on the TgDCX148-243 crystal structure

Homology models for TaDCX, PfDCX, VbDCX1, VbDCX3, CvDCX1, and CvDCX3 were obtained using Robetta (robetta.org) with the TgDCX structure as the top template and comparative models generated using the RosettaCM protocol (Song et al., 2013). As the sequence homology to their respective paralog is greater than 80%, CvDCX2 and VbDCX2 were threaded with Modeller against the Robetta coordinates for CvDCX3 and VbDCX3, respectively, and the models thus obtained were energy minimized against the Amber force field with 100 steps of steepest descent followed by 10 steps of conjugate gradient minimization (Webb and Sali). Electrostatic potential maps were calculated with APBS and displayed on the molecular surface with UCSF Chimera, with the ±10 kT/e potential isocontours shown as blue and red (Baker et al., 2001; Pettersen et al., 2004). Prior to electrostatic potential calculations, the human DCX-N structure (PDB:5IOI) was altered in UCSF Chimera by replacing the mutated residues D134-D135 with native lysines using the Dunbrack rotamers library (Burger et al., 2016; Dunbrack, 2002). The orientation relative to tubulin of the TgDCX and human DCX-C (PDB:5IP4) structures and homology models was estimated by superimposing the coordinates on the human DCX-N structure in complex with tubulin (PDB: 4ATU) (Liu et al., 2012).

ACKNOWLEDGEMENTS:

We thank Drs. John Daum and Gary Gorbsky (Oklahoma Medical Research Foundation, Oklahoma City, OK) for the EGFP-tubulin *Xenopus* S3 cell line, Dr. Richard Day (Indiana University School of Medicine, Indianapolis, IN) for the pmNeonGreen-N1 plasmid, Dr David Walliker for *Plasmodium falciparum*-3D7A genomic DNA (obtained through BEI Resources, NIAID, NIH), Yulia Pivovarova (Max F. Perutz Laboratories, Vienna, Austria) and Dr. Christopher Nosala (Indiana University) for insightful discussions, Dr. Amanda Rollins and Qing Zhang for technical support. We thank Christiane Hassel of the Indiana University Bloomington (IUB) Flow Cytometry Core Facility for assistance with flow cytometry, Dr. James Powers of the IUB Light Microscopy Imaging Facility for assistance and support with light microscopy (NIH S10-RR028697), and Drs. Barry Stein and Che-Yen Wang of the IUB Electron Microscopy Center for technical support and advice with electron microscopy. This study was supported by funding from the American Heart Association (Postdoctoral Fellowship, 18POST34090005) awarded to JML, NIH-NIAID (R01-AI132463) and the March of Dimes (6-FY18-674) awarded to KH, and facility funding from the Indiana Clinical and Translational Sciences Institute to KH, funded in part by grants #UL1 TR001108 and #TL1TR001107 from the National Institutes of Health, National Center for Advancing Translational Sciences, Clinical and Translational Sciences Award. This project has also been funded in part with Federal funds from the NIH-NIAID under Contract No.: HHSN272201700059C.

FIGURE LEGENDS

Figure 1. Conoid architecture and endogenous TgDCX localization

(A) Diagram of the *T. gondii* cytoskeleton [from (Nagayasu et al., 2016)], in which several tubulin containing structures (22 cortical microtubules, 2 intra-conoid microtubules, and 14 conoid fibers) are highlighted in red. EM images of a cross-section of each of those polymers are also shown (Hu et al., 2002). Shown in brown are several rings mentioned later in the text. The apical polar ring is the origin of the 22 cortical microtubules. A complex structure (the preconoidal rings, unlabeled), rich in intricate detail, lying at the apical end of the conoid, is portrayed in this cartoon as two featureless rings. IMC: Inner Membrane Complex. Right: a replicating parasite, with daughter parasites being built inside the mother. The cortical microtubules of the adult are omitted for clarity.

(B-D) Z-projections of SIM images of mCherryFP-TgDCX (*red*, "K-in mCh-TgDCX") knock-in parasites expressing mNeonGreenFP-β1-tubulin (*green*, mNe-TgTub) . (B) Two interphase adult parasites. One adult is outlined with a dashed white border. The arrowhead indicates the apical complex of one parasite, shown 1.5X enlarged and contrast enhanced in the inset. Tubulin and TgDCX are co-localized in the conoid, appearing as an annulus with a ~ 0.2 μm central opening. (C) Two dividing parasites at an early stage of daughter formation, with two daughters in each adult. One of the developing daughter's apical complex is indicated by the arrowhead, and enlarged 1.5X in the inset. (D) Parasites at a later stage of daughter formation. The daughter apical complexes (*white arrowhead*) are nearly mature, and daughter cortical microtubules have grown to ~ 1/3 of their length in the adult.

(E-G) EM images of the conoid region of negatively stained whole-mount *mCherryFP-TgDCX* knock-in (E, "K-in mCh-TgDCX"), *TgDCX* knockout (F, "ΔTgDCX") parasites (two images), and a complemented line generated by transfecting the *TgDCX* knockout parasite with a plasmid driving expression of TgDCX-EGFP (G, "Comp"). The conoids are shorter, distorted, and disordered in the *TgDCX* knockout parasites (F) compared to their parental strain in (E), but supplying TgDCX completely restores conoid structure (G).

Figure 2. Electron microscope (EM) images of conoids isolated from wild-type, *mCherryFP-TgDCX* knock-in and *TgDCX* knockout parasites

(A) CryoEM image of disassembled apical complexes from wild-type ("WT") parasites. Several groups of conoid fibers ("*CF*", *arrowheads*) and fragments of cortical microtubules ("*MT*", arrows) are seen. Note that the cortical microtubules are straight, whereas the conoid fibers are uniformly curved. The conoid fibers appear to become wider along their length, and their protofilaments become clearer, indicating a twist in the fibers, as diagrammed in the cartoon. The cartoon shows a cluster of fibers similar to those in the upper left of the cryoEM image. The arrow shows the direction of view in the EM image, and the boxes contain cross-sections of the fiber at the indicated locations. At the apical end of the fibers (towards the right in the cartoon and image), the direction of view yields a narrow fiber with protofilaments obscured by superposition. As the fiber twists along its length, its profile becomes wider, and there is decreasing superposition of protofilaments, giving the splayed appearance at the fiber ends.

(B) End on (left) and side views (right) of negatively stained isolated conoids from *mCherryFP-TgDCX* knock-in parasites ("K-in mCh-TgDCX"). In the left image, the apical polar ring with stumps of broken cortical microtubules encircles the conoid. On the right, the two intra-conoid microtubules are seen projecting through the conoid.

(C) Three examples of disassembled conoids isolated from *mCherryFP-TgDCX* knock-in parasites ("K-in mCh-TgDCX"). All 14 of the fibers that formed each conoid are seen. Arrows: preconoidal rings

(D) End on views of conoids isolated from *TgDCX* knockout parasites ("ΔTgDCX"). The conoids are encircled by the apical polar ring with attached fragments of cortical microtubules. Isolated conoid fibers were never observed in preparations from the *TgDCX* knockout parasite.

Figure 3. FP-tagged TgDCX generates and stabilizes curved microtubules in a heterologous system, *Xenopus laevis* S3 cells.

(A) Deconvolved wide-field images of *Xenopus* S3 cells expressing EGFP-α-tubulin (*green*) and TgDCX-mCherryFP (*red*), showing that TgDCX-mCherryFP is localized to EGFP-α-tubulin containing fibers. TgDCX-mCherryFP expression drives the formation of curved fibers, many of which are short and share similar curvatures. The area within the dashed outlines are enlarged

1.5X in the small white boxes.

(B) Fluorescence and DIC images of a small region from a different transfected cell, enlarged 2.5X relative to (A), contrast enhanced to show microtubules on the cell periphery with lower TgDCX-mCherryFP signal, following the meandering trajectory of normal cytoplasmic microtubules. .

(C) Deconvolved wide-field images of *Xenopus* S3 cells expressing EGFP-α-tubulin (*green*) and mCherryFP-TgDCX (*red*), showing that, similar to TgDCX-mCherryFP, mCherryFP-TgDCX expression drives the formation of curved fibers. Arrows indicate microtubule bundles coated with mCherryFP-TgDCX. Note the fibers containing EGFP-tubulin only in the neighboring untransfected cell, which follow the meandering, gently curved, paths of typical cytoplasmic microtubules. Insets: 1.5X

(D) Deconvolved wide-field images of *Xenopus* S3 cells expressing EGFP-α-tubulin (*green*) and mCherryFP-TgDCX (*red*) before (*upper row*) and after (*lower row*) treatment with 16 μM nocodazole for 65 min. Note that the curved fibers coated with mCherryFP-TgDCX are resistant to depolymerization by nocodazole. Arrows indicate untransfected cells, expressing EGFP-α-tubulin only, in which virtually all microtubules have depolymerized.

Figure 4. The DCX domain alone does not support stable microtubule binding in *Xenopus*, or conoid targeting in *Toxoplasma*.

(A-B) Deconvolved wide-field images of *Xenopus* S3 cells expressing EGFP-tubulin (*green*) and either mCherryFP-TgDCX148-243 (A, *red*) or mCherryFP-TgDCX71-243 (B, *red*). The boxed insets in (B) show 1.5X enlarged and contrast-enhanced small regions over the nucleus where individual arcs are more clearly seen.

(C-D) Deconvolved wide-field images of the parental RH*Δku80Δhx* ("WT") and TgDCX knockout ("ΔTgDCX") parasites expressing either mCherryFP-TgDCX148-243 (C), or mCherryFP-TgDCX71-243 (D). Arrowheads in (C) indicate the nucleus. Arrows in (D) point to the conoid; arrowhead in (D) points to a daughter conoid

(E-H) EM images of the conoid region of negatively stained *T. gondii*. Parental RH*Δku80Δhx* (E, "WT"); *TgDCX* knockout (F, "ΔTgDCX"); knockout parasites transfected with a plasmid expressing either EGFP tagged full-length TgDCX (G, "ΔTgDCX/TgDCX"), or mCherryFP-

TgDCX71-243 (H, "ΔTgDCX/TgDCX71-243"), both expressed under control of the (constitutive) *T. gondii* α-tubulin promoter (See Figure 7D).

(I) Plaque assays (see *Methods*) of the parasite strains used for (E-H); the parental *T. gondii*, *TgDCX*-knockout parasites, and knockout parasites complemented with full-length TgDCX or the fragment containing only the P25α and DCX domains, TgDCX71-243. Annotations are the same as (E-H).

Figure 5. Sequence and structure conservation among DCX domains of TgDCX orthologues.

(A) Sequences of DCX domains from *Toxoplasma gondii*, *Vitrella brassicaformis*, *Chromera velia*, *Trichoplax adhaerens*, N- and C-terminal domains of humans doublecortin, and a consensus DCX domain from the NCBI Conserved Domain Database (CD01617), were aligned using the MUSCLE program accessed through JalView (V2.10.5, http://www.jalview.org) with default parameters and displayed colored by polarity. Yellow: non-polar (G, A, V, L, I, F, W, M, P); Green: polar, uncharged (S, T, C, Y, N, Q); Red: polar, acidic (D, E); Blue: polar, basic (K, R, H). Secondary structure elements in TgDCX (beta sheet, "β"; alpha helix, "α"; turns, "T"; and a short stretch of 3_{10} helix), derived from our X-ray crystal structure (PDB 6B4A) of TgDCX148-243, are indicated above the alignment. Black arrowheads indicate residues discussed in the text (TgDCX R152 and HsDCX-N K53; TgDCX D201). CvDCX1 (EupathDB ID: Cvel_6797), CvDCX2 (EupathDB ID: Cvel_18664), CvDCX3 (EupathDB ID: Cvel_28653), VbDCX1 (EupathDB ID: Vbra_15441), VbDCX2 (EupathDB ID: Vbra_12248), VbDCX3 (EupathDB ID: Vbra21191), PfDCX (EupathDB ID: PF3D7_0517800), TaDCX (Uniprot ID: B3RTF1) and HsDCX (NG_011750).

(B) Superposition of backbone ribbon traces of TgDCX148-243 (dark gray-green; X-ray, 6B4A) on the N-terminal DCX domain of human doublecortin (yellow-orange; solution NMR, 1MJD, #11) docked with the structure of αβ-tubulin (α-tubulin blue, β-tubulin cyan; electron crystallography, 1JFF) onto the cryoEM map of human doublecortin bound to microtubules (4ATU). The DCX domain binds in the groove between protofilaments, making contacts with two αβ-dimers. Side-chains are shown for some of the surface-exposed residues that, when mutated, give rise to lissencephaly or double cortex syndrome in humans (HsDCX-N:TgDCX; Y64:H163; R76:R172; R78:K176; D86:Q184; R102:R197). The view is from the outside of the

microtubule, corresponding to Figure 2C of (Fourniol et al., 2010). The (+)-end of the microtubule is towards the top.

(C) Backbone ribbon threading of apicortin orthologue sequences onto the superimposed experimentally-determined structures of human DCX-N docked on microtubules (4ATU) and TgDCX148-243 (6B4A). The view is from the outside of the microtubule. The structures are rotated 135 degrees clockwise relative to the orientation shown in (B). The microtubule (+)-end points toward the bottom right corner of the diagram. Only the portion of one β-tubulin close to the DCX domain is included. Side chains are shown for the electronegative patch on β-tubulin, close to DCX, identified as contact region #3 on β-tubulin by (Fourniol et al., 2010). Side-chains of the residues discussed in the text, K53 on HsDCX-N and R152 on TgDCX are also shown, pointing away from tubulin in these structures.

(D) Molecular surfaces of structures and models. For the left member of each pair, the surface shown is the side closest to the microtubule surface (*i.e.*, the view from the lumen of the microtubule). For the right member of each pair, the surface shown is the side facing away from the microtubule surface. Surfaces are colored by their ABPS electrostatic potential (on a red-green-blue scale, from more negative to more positively charged). The area potentially interacting with the "site 3" reported in (Fourniol et al., 2010), a negative patch on β -tubulin, is on the Southwest corner of the left member of each pair.

Figure 6. Microtubule binding in *Xenopus* S3 cells by TgDCX and its orthologues.

(A-I) Deconvolved wide-field images of *Xenopus* S3 cells expressing both EGFP-tubulin and mCherryFP tagged DCX orthologues. The grayscale images show the fluorescence from the mCherryFP-tagged orthologues only. For the area within the smaller white boxes, both channels are displayed (*larger white boxes*) to demonstrate colocalization of the EGFP (*green*) and mCherryFP (*red*) fluorescence. For the four orthologues that do not appear to bind to microtubules (VbDCX2, VbDCX3, CvDCX2, CvDCX3), low magnification overviews of entire cells are also shown (*yellow boxes*).

Figure 7. Localization of TgDCX and its orthologues in *Toxoplasma*

(A-B) Deconvolved wide-field images of dividing *TgDCX* knockout (A, "ΔTgDCX", two examples) and RH*Δku80Δhx* (B, "WT") parasites transiently expressing TgDCX-eGFP from the *T. gondii* α-tubulin promoter. TgDCX-eGFP is highly enriched in the mother conoid (*green arrowhead*) and daughter conoids (*green arrows*) and is absent from the cortical microtubules of mother parasites. However, in contrast to expression regulated by the endogenous promoter, when expression is driven by this nearly constitutive α1-tubulin promoter (See D), in some cases TgDCX-eGFP signal is also detected on the daughter cortical microtubules, centrosomes (*cyan arrowheads*), and basal complexes (*cyan arrows*). Dashed cyan lines in (A) outline two of four parasites in the same parasitophorous vacuole. Insets: 1.5X. The lower panels show merged DIC and fluorescence (in red) images.

(C) Deconvolved wide-field images of the RH*Δku80Δhx* (WT) parasites expressing FP tagged DCX orthologues. Note that among the eight orthologues, only CvDCX1 closely mimics the pattern of localization shown by TgDCX (when expressed under this *T. gondii* α1-tubulin promoter). *Green arrows*: daughter conoids. *Green arrowheads*: mother conoids. *Cyan arrowhead*: centrosome. Inset: 1.5X

(D) Time course of RNA expression levels (Behnke et al., 2010) in *Toxoplasma gondii* for α1-tubulin (*green*) and TgDCX (*red*). Tubulin expression is nearly constitutive, whereas TgDCX varies by more than 30-fold across the cell-cycle.

Figure 8. CvDCX1 cannot rescue the structural and lytic cycle defects of the TgDCX knockout parasite.

(A-C) EM images of the conoid region of negatively stained *T. gondii*. Parental RH*Δku80Δhx* (A, "WT"), *TgDCX* knockout (B, "ΔTgDCX", two examples); knockout parasites transfected with a plasmid expressing CvDCX1-mNeonGreenFP expressed under control of the *T. gondi*i α-tubulin promoter (C, "ΔTgDCX/CvDCX1", three examples). Compare with Fig. 4G and H.

(D) Plaque assay (see *Methods*). Knockout parasites complemented with TgDCX-eGFP expressed under control of the *T. gondii* α-tubulin promoter ("ΔTgDCX/TgDCX"). Other annotations as in (A-C). Compare with Fig. 4I.

Figure 9. Correlative light and electron microscopy analysis of microtubules in *Xenopus* cells expressing CvDCX1

(A) EM images of microtubules in sections of an untransfected *Xenopus* cell. In all cases where they are countable, 13 protofilaments (pf) are present. No microtubules with other than 13 pf were seen in untransfected cells.

(B) Fluorescence and DIC light microscope images of the cell sectioned in (A). The cell is from a line expressing EGFP-α-tubulin. The plane of sectioning in the EM images is shown by the white bar.

(C) EM images of microtubules from sections of a *Xenopus* cell transfected with mCherryFP-CvDCX1. All microtubules have 13 pf. The tannic-acid-enhancement of microtubule staining (see *Methods*) is more effective when the microtubules are heavily decorated, which makes the protofilaments more obvious and more easily countable, but the diameter of the microtubules is approximately the same as in untransfected cells.

(D) Fluorescence and DIC light microscopy images of the cell sectioned in (C). mCherryFP-CvDCX1 is shown in red, EGFP-α-tubulin in green. The plane of section is shown by the white bar. The magnification is the same as for (B). Note that the elongated narrow extension of the transfected cell lies on top of another untransfected cell, running over the edge of the latter's nucleus.

(E) Low magnification EM cross-section images of the cell shown in D. The thin extension of the transfected cell is seen crossing over the underlying untransfected cell. The region within the white box, shown enlarged on the right, contains >100 parallel microtubules viewed in cross-section, appearing as tiny black doughnuts at this magnification.

Figure 10. Correlative light and electron microscopy analysis of microtubules in *Xenopus* cells expressing TgDCX.

(A) Montage of images of microtubule rafts viewed in cross-section by EM, from a *Xenopus* cell expressing TgDCX-mCherryFP. Often the microtubules on one edge of a raft are incomplete tubes (*white arrows*), as are some of the single microtubules in these cells. The light micrographs at the bottom show fluorescence and DIC images of the sectioned cell, which is also expressing EGFP-α-tubulin. The plane of sectioning is shown by the white bar. TgDCX-

mCherryFP is shown in red, EGFP-α-tubulin in green.

(B) Light and electron microscope images of a *Xenopus* cell expressing mCherryFP-TgDCX71-243 and EGFP-α-tubulin. mCherryFP-TgDCX71-243 is shown in red, EGFP-α-tubulin in green. The plane of section is indicated by the white bar. The EM images show microtubule cross-sections in these cells, which are similar to those in cells expressing full-length TgDCX, quite different from microtubules in untransfected cells.

(C) Comparison of microtubule shapes and sizes. *Top two images*: a single microtubule with more than 13 pf, and a cluster of three microtubules from TgDCX71-243 transfected cells. Note that the width of the incomplete microtubules is often larger than the complete tubes, suggesting that the gap results from a tube expanding in diameter and splitting, rather than from loss of protofilaments. *Third image from the top*: a 13 pf microtubule from a cell expressing CvDCX1. *Bottom image*: a 13 pf microtubule from an untransfected cell.

Figure 11. Diagram illustrating the changing geometry of the TgDCX-containing fibers of the conoid.

Extension of the conoid through the apical polar ring, which occurs as the parasites reactivate motility and exit their lysed host cell, is accompanied by a change in conoid shape from more conical to more cylindrical. The change in fiber arrangement can be visualized as a decrease in the diameter at the base of the conoid with concurrent clockwise (viewed from the apical end) rotation of the base with respect to the apex, thus partially "unwinding" the left-handed spiral of the conoid fibers. The consequence of this "unwinding" for fibers anchored at their ends, as the conoid fibers seem to be, is introduction of a right-handed twist along the length of each individual fiber. Sagittal sections of the conoid in intact parasites (Hu et al., 2002) show that in the extended state, the conoid fibers all have the same rotational orientation (lower half of the Figure). A sagittal section cuts each fiber at a different location along its length, from closer to their apical end for the fibers at the top of the section, to near the basal end of fibers at the bottom of the section. Thus, the observed identical rotational orientations of the fibers at the top and bottom demonstrates that the fibers have little or no twist in the extended conoid. This implies that they have a left-handed twist in the retracted conoid, as illustrated in the upper half of the Figure. For clarity, the change in fiber orientation has been exaggerated in the diagram.

Note also that the diagrams here are oversimplified for clarity: in the untilted sagittal section as diagrammed, the fiber profiles cannot be clearly seen. In order to make the profiles visible, the section must be tilted in the microscope by plus (to see the profiles on one side) or minus (to see the profiles on the other side) the pitch angle of the fibers. See Fig 6 in (Hu et al., 2002) for a demonstration.

Table 1. Sequence conservation and microtubule interaction properties among TgDCX and its orthologues.

Table 2: Data Collection, Phasing, and Refinement Statistics for TogoA.17199.a.B3.PW38274

Table 3. Oligonucleotides and gblock fragments used in this study

References:

Adams, P. D., Afonine, P. V., Bunkoczi, G., Chen, V. B., Davis, I. W., Echols, N., Headd, J. J., Hung, L. W., Kapral, G. J., Grosse-Kunstleve, R. W. et al. (2010). PHENIX: a comprehensive Python-based system for macromolecular structure solution. *Acta Crystallogr D Biol Crystallogr* **66**, 213-21.

Amos, L. A. and Amos, W. B. (1991). The bending of sliding microtubules imaged by confocal light microscopy and negative stain electron microscopy. *J.Cell.Sci.Suppl.* **14**, 95-101.

Aslanidis, C. and de Jong, P. J. (1990). Ligation-independent cloning of PCR products (LIC-PCR). *Nucleic acids research* **18**, 6069-74.

Baker, N. A., Sept, D., Joseph, S., Holst, M. J. and McCammon, J. A. (2001). Electrostatics of nanosystems: application to microtubules and the ribosome. *Proc Natl Acad Sci U S A* **98**, 10037-41.

Bechstedt, S. and Brouhard, G. J. (2012). Doublecortin recognizes the 13-protofilament microtubule cooperatively and tracks microtubule ends. *Developmental cell* **23**, 181-92.

Behnke, M. S., Wootton, J. C., Lehmann, M. M., Radke, J. B., Lucas, O., Nawas, J., Sibley, L. D. and White, M. W. (2010). Coordinated progression through two subtranscriptomes underlies the tachyzoite cycle of Toxoplasma gondii. *Plos One* **5**, e12354.

Bryan, C. M., Bhandari, J., Napuli, A. J., Leibly, D. J., Choi, R., Kelley, A., Van Voorhis, W. C., Edwards, T. E. and Stewart, L. J. (2011). High-throughput protein production and purification at the Seattle Structural Genomics Center for Infectious Disease. *Acta crystallographica Section F, Structural biology and crystallization communications* **67**, 1010-4.

Burger, D., Stihle, M., Sharma, A., Di Lello, P., Benz, J., D'Arcy, B., Debulpaep, M., Fry, D., Huber, W., Kremer, T. et al. (2016). Crystal Structures of the Human Doublecortin C- and N-terminal Domains in Complex with Specific Antibodies. *The Journal of biological chemistry* **291**, 16292-306.

Chaaban, S. and Brouhard, G. J. (2017). A microtubule bestiary: structural diversity in tubulin polymers. *Mol Biol Cell* **28**, 2924-2931.

Chen, V. B., Arendall, W. B., 3rd, Headd, J. J., Keedy, D. A., Immormino, R. M., Kapral, G. J., Murray, L. W., Richardson, J. S. and Richardson, D. C. (2010). MolProbity: all-atom structure validation for macromolecular crystallography. *Acta Crystallogr D Biol Crystallogr* **66**, 12-21.

Choi, R., Kelley, A., Leibly, D., Hewitt, S. N., Napuli, A. and Van Voorhis, W. (2011). Immobilized metal-affinity chromatography protein-recovery screening is predictive of crystallographic structure success. *Acta crystallographica Section F, Structural biology and crystallization communications* **67**, 998-1005.

Collaborative Computational Project, N. (1994). The CCP4 suite: programs for protein crystallography. *Acta Crystallogr D Biol Crystallogr* **50**, 760-3.

Cowtan, K. (2010). Recent developments in classical density modification. *Acta Crystallogr D Biol Crystallogr* **66**, 470-8.

Davis, C. and Gull, K. (1983). Protofilament number in microtubules in cells of two parasitic nematodes. *Journal of Parasitology* **69**, 1094-9.

Desser, S. S., Baker, J. R. and Lake, P. (1970). The fine structure of Leucocytozoon simondi. I. Gametocytogenesis. *Can J Zool* **48**, 331-6.

Dunbrack, R. L., Jr. (2002). Rotamer libraries in the 21st century. *Curr Opin Struct Biol* **12**, 431-40.

Dustin, P. (1984). Microtubules. Berlin: Springer-Verlag.

Emsley, P., Lohkamp, B., Scott, W. G. and Cowtan, K. (2010). Features and development of Coot. *Acta Crystallogr D Biol Crystallogr* **66**, 486-501.

Ettinger, A., van Haren, J., Ribeiro, S. A. and Wittmann, T. (2016). Doublecortin Is Excluded from Growing Microtubule Ends and Recognizes the GDP-Microtubule Lattice. *Current biology : CB* **26**, 1549-1555.

Fourniol, F. J., Sindelar, C. V., Amigues, B., Clare, D. K., Thomas, G., Perderiset, M., Francis, F., Houdusse, A. and Moores, C. A. (2010). Template-free 13-protofilament microtubule-MAP assembly visualized at 8 A resolution. *The Journal of cell biology* **191**, 463-70.

Gleeson, J. G., Lin, P. T., Flanagan, L. A. and Walsh, C. A. (1999). Doublecortin is a microtubule-associated protein and is expressed widely by migrating neurons. *Neuron* **23**, 257-71.

Grosse-Kunstleve, R. W. and Adams, P. D. (2003). Substructure search procedures for macromolecular structures. *Acta Crystallogr D Biol Crystallogr* **59**, 1966-73.

Haimo, L. T. and Rosenbaum, J. L. (1981). Cilia, flagella, and microtubules. *The Journal of cell biology* **91**, 125s-130s.

Heaslip, A. T., Dzierszinski, F., Stein, B. and Hu, K. (2010). TgMORN1 is a key organizer for the basal complex of Toxoplasma gondii. *PLoS Pathogens* **6**, e1000754.

Heiges, M., Wang, H., Robinson, E., Aurrecoechea, C., Gao, X., Kaluskar, N., Rhodes, P., Wang, S., He, C. Z., Su, Y. et al. (2006). CryptoDB: a Cryptosporidium bioinformatics resource update. *Nucleic acids research* **34**, D419-22.

Hlavanda, E., Kovacs, J., Olah, J., Orosz, F., Medzihradszky, K. F. and Ovadi, J. (2002). Brain-specific p25 protein binds to tubulin and microtubules and induces aberrant microtubule assemblies at substoichiometric concentrations. *Biochemistry* **41**, 8657-64.

Hu, K., Johnson, J., Florens, L., Fraunholz, M., Suravajjala, S., DiLullo, C., Yates, J., Roos, D. S. and Murray, J. M. (2006). Cytoskeletal components of an invasion machine – the apical complex of *Toxoplasma gondii*. *PLoS Pathogens* **2**, 0121-0139.

Hu, K., Roos, D. S. and Murray, J. M. (2002). A novel polymer of tubulin forms the conoid of Toxoplasma gondii. *The Journal of cell biology* **156**, 1039-50.

Kabsch, W. (2010). Xds. *Acta Crystallogr D Biol Crystallogr* **66**, 125-32.

Langer, G., Cohen, S. X., Lamzin, V. S. and Perrakis, A. (2008). Automated macromolecular model building for X-ray crystallography using ARP/wARP version 7. *Nat Protoc* **3**, 1171-9.

Liu, J. S., Schubert, C. R., Fu, X., Fourniol, F. J., Jaiswal, J. K., Houdusse, A., Stultz, C. M., Moores, C. A. and Walsh, C. A. (2012). Molecular basis for specific regulation of neuronal kinesin-3 motors by doublecortin family proteins. *Molecular cell* **47**, 707-21.

McCoy, A. J., Grosse-Kunstleve, R. W., Adams, P. D., Winn, M. D., Storoni, L. C. and Read, R. J. (2007). Phaser crystallographic software. *J Appl Crystallogr* **40**, 658-674.

Mondragon, R. and Frixione, E. (1996). Ca(2+)-dependence of conoid extrusion in Toxoplasma gondii tachyzoites. *J. Eukaryotic Microbiol.* **43**, 120-7.

Moores, C. A., Perderiset, M., Francis, F., Chelly, J., Houdusse, A. and Milligan, R. A. (2004). Mechanism of microtubule stabilization by doublecortin. *Molecular cell* **14**, 833-9.

Murray, J. M. (2017). An icosahedral virus as a fluorescent calibration standard: a method for counting protein molecules in cells by fluorescence microscopy. *J Microsc* **doi: 10.1111/jmi.12559**.

Nagayasu, E., Hwang, Y.-c., Liu, J., Murray, J. and Hu, K. (2016). Loss of a doublecortin (DCX) domain containing protein causes structural defects in a tubulin-based organelle of *Toxoplasma gondii* and impairs host cell invasion. *Molecular Biology of the Cell* **E16-08-0587**

Orosz, F. (2009). Apicortin, a unique protein, with a putative cytoskeletal role, shared only by apicomplexan parasites and the placozoan Trichoplax adhaerens. *Infect Genet Evol* **9**, 1275-86.

Orosz, F. (2016). Wider than Thought Phylogenetic Occurrence of Apicortin, A Characteristic Protein of Apicomplexan Parasites. *J Mol Evol* **82**, 303-14.

Orosz, F. (2018). Does apicortin, a characteristic protein of apicomplexan parasites and placozoa, occur in Eumetazoa? *Acta Parasitol* **63**, 617-633.

Patra, K. P. and Vinetz, J. M. (2012). New ultrastructural analysis of the invasive apparatus of the Plasmodium ookinete. *The American journal of tropical medicine and hygiene* **87**, 412-7.

Pettersen, E. F., Goddard, T. D., Huang, C. C., Couch, G. S., Greenblatt, D. M., Meng, E. C. and Ferrin, T. E. (2004). UCSF Chimera--a visualization system for exploratory research and analysis. *J Comput Chem* **25**, 1605-12.

Portman, N., Foster, C., Walker, G. and Slapeta, J. (2014). Evidence of intraflagellar transport and apical complex formation in a free-living relative of the apicomplexa. *Eukaryotic Cell* **13**, 10-20.

Read, R. J. and McCoy, A. J. (2011). Using SAD data in Phaser. *Acta Crystallogr D Biol Crystallogr* **67**, 338-44.

Roos, D. S., Donald, R. G., Morrissette, N. S. and Moulton, A. L. (1994). Molecular tools for genetic dissection of the protozoan parasite *Toxoplasma gondii*. *Methods Cell Biol.* **45**, 27-78.

Rufer, A. C., Kusznir, E., Burger, D., Stihle, M., Ruf, A. and Rudolph, M. G. (2018). Domain swap in the C-terminal ubiquitin-like domain of human doublecortin. *Acta Crystallogr D Struct Biol* **74**, 450-462.

Shaner, N. C., Campbell, R. E., Steinbach, P. A., Giepmans, B. N., Palmer, A. E. and Tsien, R. Y. (2004). Improved monomeric red, orange and yellow fluorescent proteins derived from Discosoma sp. red fluorescent protein.[see comment]. *Nature Biotechnology* **22**, 1567-72.

Shaner, N. C., Lambert, G. G., Chammas, A., Ni, Y., Cranfill, P. J., Baird, M. A., Sell, B. R., Allen, J. R., Day, R. N., Israelsson, M. et al. (2013). A bright monomeric green fluorescent protein derived from Branchiostoma lanceolatum. *Nat Methods* **10**, 407-9.

Song, Y., DiMaio, F., Wang, R. Y., Kim, D., Miles, C., Brunette, T., Thompson, J. and Baker, D. (2013). High-resolution comparative modeling with RosettaCM. *Structure* **21**, 1735-42.

Taylor, K. R., Holzer, A. K., Bazan, J. F., Walsh, C. A. and Gleeson, J. G. (2000). Patient mutations in doublecortin define a repeated tubulin-binding domain. *The Journal of biological chemistry* **275**, 34442-50.

Webb, B. and Sali, A. Comparative Protein Structure Modeling Using MODELLER.

Table 1. Sequence conservation and microtubule interaction properties among TgDCX and its orthologues.

orthologue (size, aa)	DCX domain (identical/positive,%)	P25α-DCX domain (identical/similar,%)	P25α to DCX (aa)[1]	N-term. extension[2] (aa)	Toxo location[3]	Xenopus[4]
TgDCX (256)	(100/100)	(100/100)	44	62	A,D,T	B,B,B
CvDCX1 (213)	46/65	50/60	44	31	A,D,T	B,B
CvDCX2 (174)	33/54	36/52	38	4	a,D,C	b
CvDCX3 (175)	32/53	35/52	38	3	a,D,C	
VbDCX1 (190)	48/71	47/63	39	14	a,D,c[5]	B,B
VbDCX2 (168)	39/56	39/53	45	8	a,D,C	
VbDCX3 (184)	39/56	41/56	45	0	a,D,C	b
PfDCX (238)	45/71	36/56	35	83	a,D,C	B,B
TaDCX (178)	34/53	36/51	38	7	C	b

1: The partial P25α domains span ~50 aa, the DCX domains ~ 80 aa.
2: Length of sequence preceding the P25α domain
3: Localization in *Toxoplasma* of the protein when expressed under control of the α-tubulin promoter is specified as: **A**, adult (mother) conoid strongly; **a**, adult conoid weakly; **D**, daughter conoid; **T**, daughter cortical MT; **C** or **c**, bright or dim diffuse cytoplasmic.
4: Localization in *Xenopus* is specified as: B or b, binds to microtubules prominently or weakly; B,B, binds to and bundles microtubules; B,B,B, binds, bundles, and bends microtubules
5: Also prominent mitochondrial localization

Table 2: Data Collection, Phasing, and Refinement Statistics for TogoA.17199.a.B3.PW38274

Parameters	**Iodide**	**Native**
Wavelength (Å)	1.5418	1.5418
Space Group	$P2_12_12_1$	$P2_12_12_1$
Cell Dimensions		
a, b, c (Å)	36.40, 53.28, 96.25	36.86, 53.23, 96.38
α, β, γ (°)	90.000, 90.000, 90.000	90.000, 90.000, 90.000
Resolution (Å)	50.00-2.00	50.00-2.00
R_{merge} (%)	4.5 (14.4)	5.9 (55.7)
$I/\sigma I$	44.1 (14.2)	18.0 (2.7)
Completeness (%)	98.7 (88.5)	99.8 (99.8)
Redundancy	14.0 (8.5)	6.1 (3.9)
Refinement		
Resolution (Å)		35.7-2.0
Reflections (#)		13372
R_{work}/R_{free} (%)		18.6/26.1
Number of Non-Hydrogen Atoms		
Protein		1463
Formate		6
Water		104
R_{msds}		
Bond Lengths (Å)		0.007
Bond Angle (°)		0.784
Average B Factors (Å^2)		
Overall		45.67
Protein		45.59
Formate		55.3
Water		45.29

Table 3. Oligonucleotides and gBlock fragments used in this study

name	sequence
S1	GGAGGAACAGGATCTGGTGGAACTGGTTCTGGTGGTTCAGTGAGCAAGGGCGAG
AS1	GCAGCTTCTGTTTACTTAAGCTACTTGTACAGCTCGTCC
CvDCX1_gBlock	gaattccctttagatccgctagcaaaATGGAGTATTTGCGATACGATGAGAGGCCGGCGGCAGT GCCGGGTCCCTCTACCAACGCAATACAGAACCCGTACAACACAAACCACGTGATGC AGGGAGAGTACGGGTTTGAAGAGCCCTCTGTATGGGAGAGGCTCACAGATCCGTC CAGGTATACAGGGGTGCACAGAGAGCGATTTGATGAGTTTGGTCGTGGGCGAGGTC TAGCAGGGCGGGAGAACGTGTACTACTTCGATGGGATGACGGAGAGTCCCTCGAG GTGTCACGAGATCTACTCGACCGTGGTCACACAAAAACGAAAGGCCGCTGTCACAC CAGGAACCCTGGGGGTTCAAAAGTTCGGAACCCAGGCAGTGACCCCCAAGTTGAT CTGGGTGTACCGAAACGGTGACAGGTCGCACGAGGGTCACCCCGTCTACCTGCGA AATTCCATCAAGACGATGGAGTTCCTCTACAGAGAGTGCACCAAGGTGGCCTGTCC GTTCACGGGCCCTGTTTTGAAGATTTACGACCAGAATCTCAAGAGAGTGAAGAAGTT GGAGCACTTCGTTGACGGGGGGAAGTACCTATGCTGCGGGGGGGAGCTCCCCTCT CTGGACAAACTCGAGAAGTTCCTCTCGAAGTTCGTCTTTGTCATCggaggaacaggatctg
CvDCX2_gBlock	gaattccctttagatccgctagcaaaATGCCCGACGCCTTCCTTGAGAGAATGACCGACGCCTC CCAGTACACGGGAGCCCACAAAGCCCGCTTCGATGCTGACGGGAACGGCCGCGGT CTGGCCGGGAGAGAGAACGTGGTGTACTACGATGGCTCCACAGAGTCCGCAACCC GCAGCCATGCCGTCGAGAATACAGTGCAAAAGAAGGGAAATCGTAAAGCAGTTGTG ACGGGCCCTCTTGGGTGCCAGAAGTTCGGAACCCAGGCCGATACCCCCATTTCCTT CACAATCTACAAGAACGGCGACAAGTTCCACAAAGGCCACAAGATCCTTCTCAAGA AGCACTACCGCAACATGCAGCAGCTTATTGACGAGTGCAATAAGCACGCCCAGCCC CTCACCGGTCCCATCCGCCGCCTCTACCGCACGGACCTGCGAACGTGGGTGAAGG AGCTCCACGAGTTTGAGGATGGCGCCAAGTACCTGTGCGTTGCCGGAGAGCACCC GAAGGATGACATCGAGAAGATCCCCCCCGGGTTCTGGGAGggaggaacaggatctg
CvDCX3_gBlock	gaattccctttagatccgctagcaaaATGCCCAACGACGCCACCCTTGCAAGACTTACTGACAC TTCCAAGTACACGGGAGCCCACAAGCAACGTTTTGATGAGGACGGCAAAGGACGC GGTCTGGCAGGGAGGGAGAACGTCACACACCACGACGGTTCCACTGAGTCTGCTG TTCGATCACACGCAATTGAGAAGACAGTGGACGAGAAAGCACACAAGAAATCAGTT GTGAAGGGCCCCCTTGGACAACAGAAGTTCGGCACCCAGGCCGACACCCCGATCT CCTTCATGATTTACAAGAACGGGGACAAGAACCACAAGGGCCACAAGGTCCTTCTC AAGAAGCACTTCCGCAACATGCAGCAGTTGACTGATGAGTGCAACAAGCACGCGGC GCCTCTGACCGGGCCTATCCGACGTTTCTACCGTCCTGACCTGAAGACCTGGGTTA AGGACCTGACGGAGTTCGAGGACGGCGGCAAGTACCTGTGCGTTGCCGGGGAGA ACCCGAAGGACGACATTGAGAAGATCCCCCCCGGGTTTTTCGAAggaggaacaggatctg
VbDCX1_gBlock	gaattccctttagatccgctagcaaaATGGCACTTTCAAGCGCTGTCGGCCGCCACCGCAACAT ATTCGAGAAACTGTGTGATCCCTCCCTCTATACAGGAGCACATAGGGAGCGATTCGA TGAGAACGGCAAGGGCAGAGGGCTGGCGGGACGAGAATACGTGTATTACGTTGAT GGGATGACTGAGAGCCCCACGCGATGCCACGAGGTATACTCGTCTGTGAGGGAGA GACCCAAACGCAAACCGCTCAGAAGACCTCCCGCGCTCAAAGAGCGTATGTCCGG GGCACCGCCGAGGGCGAAGCTCATATGGCTGTACAGAAACGGAGACAAGAAACAC CTGGGCTCTCCCTCCTTCGTGCGGCCGCATGTGCAGTCGCTGGACCTGCTGTATC GTGAAGCGTCAGCTGAGATCCGCCTGCTCACCGGGCCGGTCAAACGTCTGTATGA CCAACATCTGGAGGCAATCAGAGACATAGACGACCTCACCGACGGCGGCAAGTATC TCTGCTGCGCCGGCGAGCAGCCATGTATGGAGAAGCTGGACCATTTCCTCTCTGAC TACGTCGTATGGCCGACTCTGCTGCACACGAGAggaggaacaggatctg

name	sequence
VbDCX2_g Block	gaattccctttagatccgctagcaaaATGTCGGGAAGGAAGAGCCCCGAGAAGCAGAGCATCTT CGACAGGCTCACCGACCACACCCAATACACGGGTGCCCATAAGCACCGTTTCGACG AGGGCGGTAAGGGGCGAGGGATTGCTGGTCGGGAGGAGCTGGTCAACATTGACG GCTCCACCGAATCTTCTGCCCGCCGCCACGCCGTGGAGAAGACAGTCGACCATGT CGAGCGTGCCGGGCGCAAGCCAGTGGTGCAGGGCGCCCTTGGCCAGCAGAAGTT CGGCACCCAAGCTGAGACACCCATCACCATTTGGCTCTACAGGAACGGTGACAAGC ACTTCAAGGGCGTCAAGTTCATCGTCAAGAAGACCATCCGGAACGTGGAACAGTTC GTTGCTGAGGCGGGCAAGTCGGGCTGCAGCCCCAAGAGCGGGGTGATCCGCAAG ATCTACAAGCAGAACATGAAGACCATCATCAAGGACATCACCGAATTCGAAGACGGC GAGAAGTACCTCTGCTGCGGAGCCGAGAAGCCCCAGGATGACCCCGAGCACATCC CTGCTGCCTTCCTCGAGggaggaacaggatctg
VbDCX3_g Block	gaattccctttagatccgctagcaaaATGGCGCCGAAGCAAAACATCTTTGACAAGCTCACCGA TAGCTCCCAATACACGGGGGCCCACAAGCACCGCTTCGACGACTCCGGCCAGGGT CGTGGCATCGCTGGGAGAGAGGAAATCGTCAACGTGGATGGTTCAACCGAGTCGA CCGCACGCAAACATGCCGTGGAGAAGACCGTCGACCACGCCGAGCGTGCGGGTC GTAAGCCAGTAGTGCAGGGGCCCCTCGGCCAGCAGAAGTTCGGGACTCAGGCGG AGACACCCATCTCCATCTGGCTGTACAAGAACGGCGACAAGCACTTCAAGGGAGTC AAGTTCGTCGTCAAGAAGACCATCAGAAACATGGACCAGTTCATCGCTGAGGCCAA CAAGCAGGGCTGCCAGCCCAAGAGCGGTGTGATTCGTAAGATCTACAAGCAGAACA TGAAGACTGTTGTCAAGGACCTGGCAGACTTCGAAGACGGCGAAAAATACCTCTGC TGTGGACCCGAGAAGCCCCAGGAGggaggaacaggatctg
S2	GAATTCCCTTTTAGATCCGCTAGCAAAATGGAGAATTTTGATGAAGTTATAAAAG
AS2	ATGGATGCTTACAAGAATTTATCTTGTGGGTCTTTTCTT
S3	AAGAAAAGACCCACAAGATAAATTCTTGTAAGCATCCAT
AS3	CAGATCCTGTTCCTCCAGTTAGAAAGTGAAGACTCAAG
S4	GAATTCCCTTTTAGATCCGCTAGCAAAATGGCGAGTAAGAAATCTCAAGA
AS4	CAGATCCTGTTCCTCCTTGGAACAGAGATGGCG
S5	GGTTCCGGTGGGTCAATTCCAGCTCCTAGATTAATGTG
AS5	GGGCAGCTTCTGTTTACTTAAGTCACTGAATCACCCATTCGC
S6	GGTTCCGGTGGGTCAAATGTTTTTGAACGGCTAACC
AS6	GGGCAGCTTCTGTTTACTTAAGTCACTGAATCACCCATTCGC
S7	GAATTCCCTTTTAGATCCGCTAGCAAAATGGTGAGCAAGGGC
AS7	TGACCCACCGGAACCAGTTCCACCAGACCCGGTACCTCCCTTGTACAGCTCGTCC A
S8	GTACAAGTCCGGACTCAGATCTATTCCAGCTCCTAGATTAATGTG
AS8	GGATCCCGGGCCCGCTTAAGTTATCACTGAATCACCCATTCGC
S9	gtacaagtccggactcagatctAATGTTTTTGAACGGCTAACC
AS9	ggatcccgggcccgcttaagttaTCACTGAATCACCCATTCGC
S10	AATTCTGCAGTCGACGCTTAAGCGGGC
AS10	CCGGGCCCGCTTAAGCGTCGACTGCAG

name	sequence
S11	CCCAAGCTGGCTAGCGTTTAAAGTTAAGC
AS11	AACGGGCCCTTAAGACTCGAG
S12	GTACAAGTCCGGACTCAGATCTGAGTATTTGCGATACGATGAGAGG
AS12	GGATCCCGGGCCCGCTTAAGTTAGATGACAAAGACGAACTTCG
S13	GTACAAGTCCGGACTCAGATCTCCCGACGCCTTCCTTG
AS13	GGATCCCGGGCCCGCTTAAGTTACTCCCAGAACCCGGGGGGG
S14	GTACAAGTCCGGACTCAGATCTCCAACGACGCCACCCTTGC
AS14	GGATCCCGGGCCCGCTTAAGTTATTCGAAAAACCCGGGGGG
S15	GTACAAGTCCGGACTCAGATCTGCGCCGAAGCAAAACATCT
AS15	GGATCCCGGGCCCGCTTAAGTTACTCCTGGGGCTTCTCGG
S16	GTACAAGTCCGGACTCAGATCTGCACTTTCAAGCGCTGTC
AS16	GGATCCCGGGCCCGCTTAAGTTATCTCGTGTGCAGCAGAGTC
S17	GTACAAGTCCGGACTCAGATCTTCGGGAAGGAAGAGCCC
AS17	GGATCCCGGGCCCGCTTAAGTTACTCGAGGAAGGCAGCAGG
S18	GTACAAGTCCGGACTCAGATCTGAGAATTTTGATGAAGTTATAAAAGAATATCAG
AS18	GGATCCCGGGCCCGCTTAAGTTAAGTTAGAAAGTGAAGACTCAAGTTTCG

Figure 1

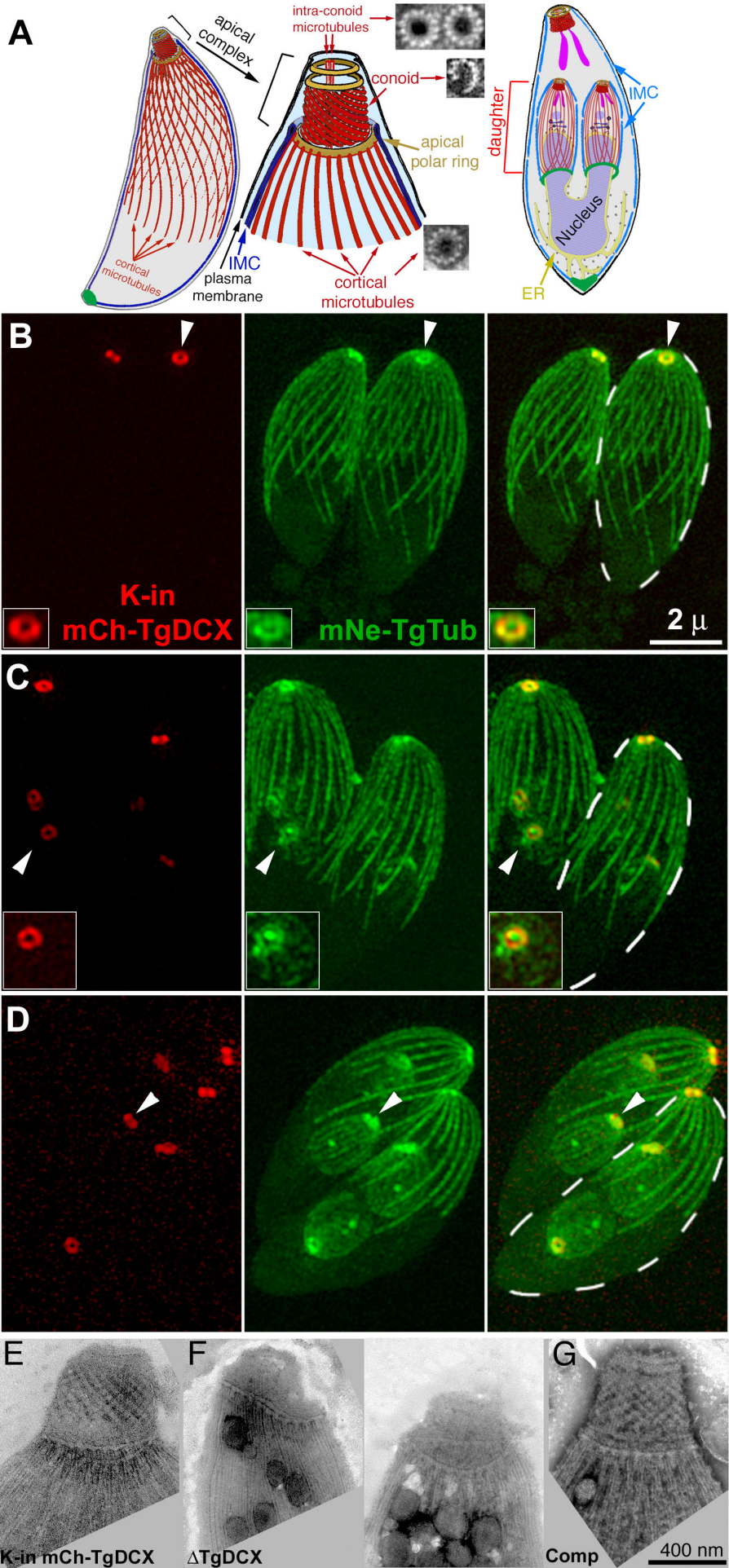
A
apical complex
intra-conoid microtubules
conoid
apical polar ring
daughter
IMC
Nucleus
ER
cortical microtubules
IMC
plasma membrane
cortical microtubules
B
K-in mCh-TgDCX
mNe-TgTub
2 μ
C
D
E
K-in mCh-TgDCX
F
ΔTgDCX
G
Comp
400 nm

Figure 2

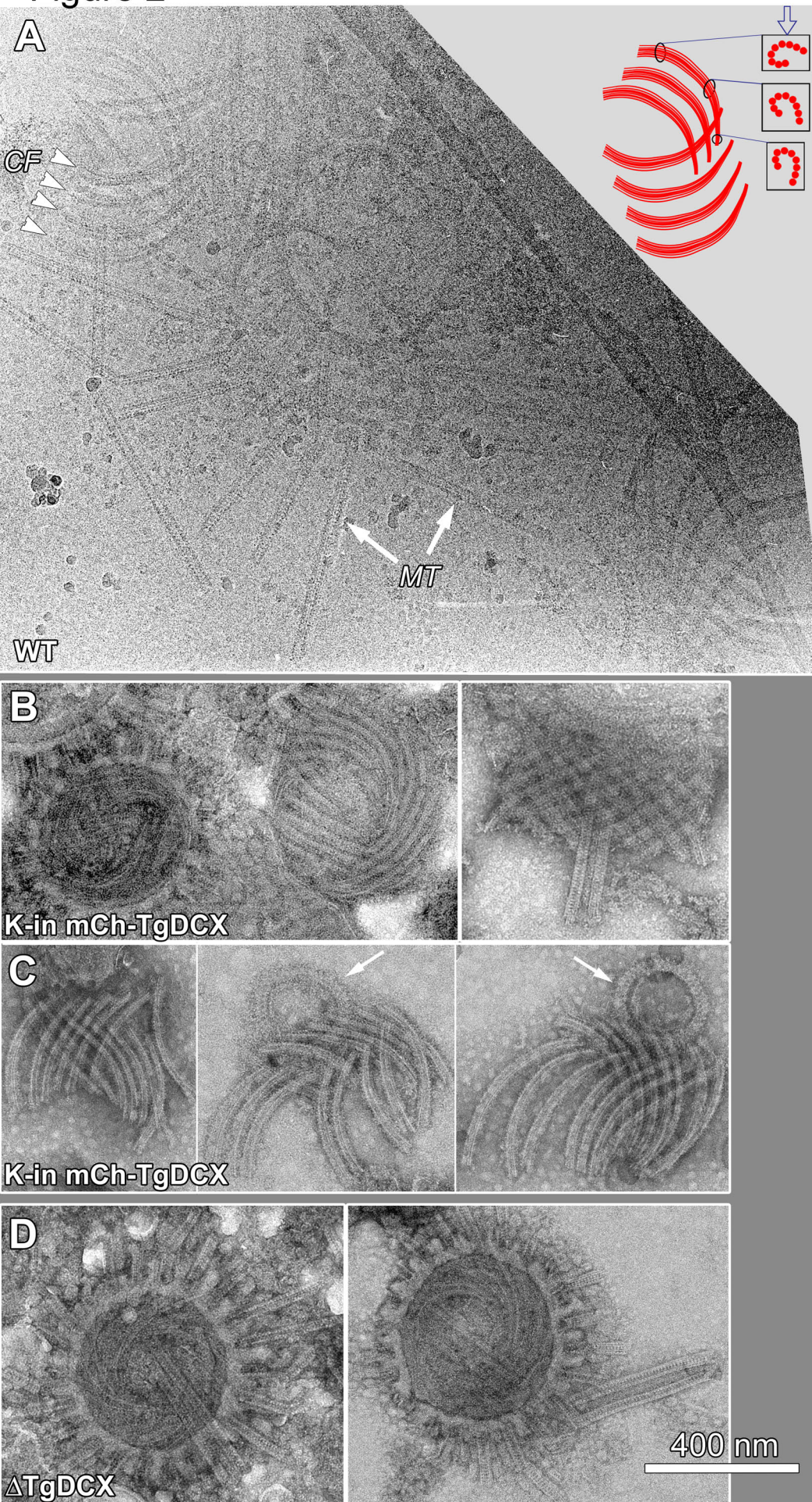

Figure 3

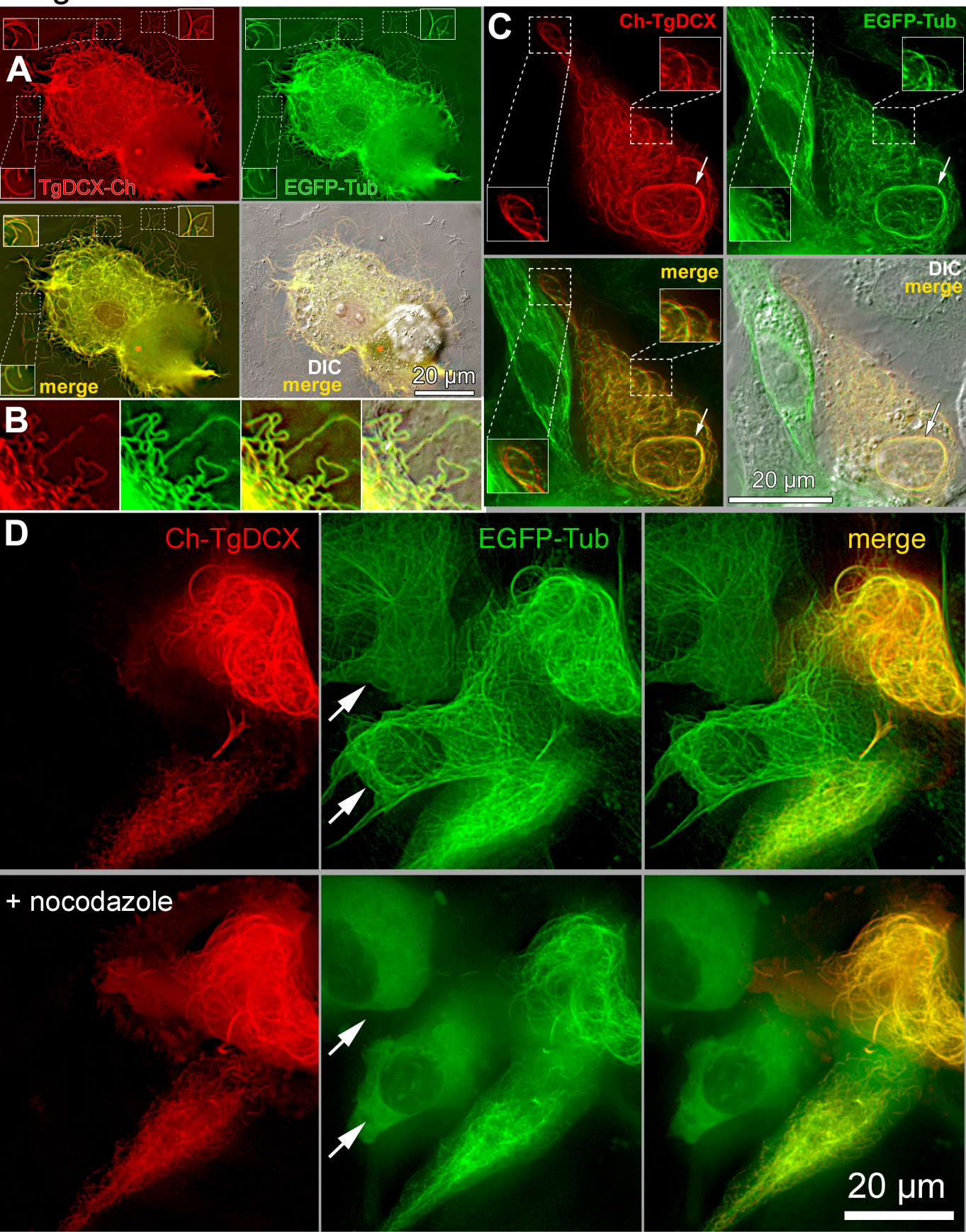
A
TgDCX-Ch
EGFP-Tub
merge
DIC
merge
20 µm
B
C
Ch-TgDCX
EGFP-Tub
merge
DIC
merge
20 µm
D
Ch-TgDCX
EGFP-Tub
merge
+ nocodazole
20 µm

Figure 4

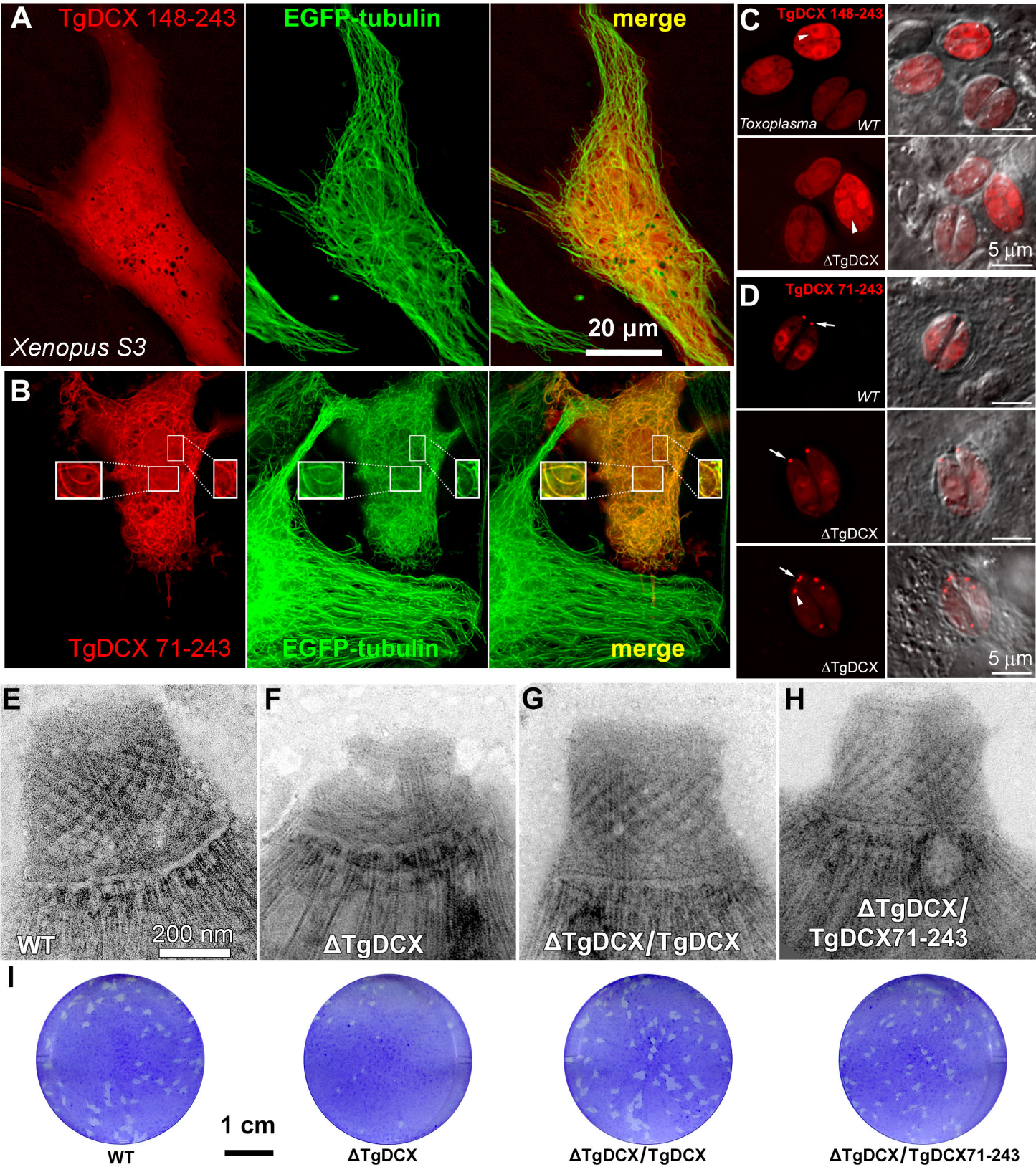
A
TgDCX 148-243
EGFP-tubulin
merge
Xenopus S3
20 µm
B
TgDCX 71-243
EGFP-tubulin
merge
C
TgDCX 148-243
Toxoplasma
WT
ΔTgDCX
5 µm
D
TgDCX 71-243
WT
ΔTgDCX
ΔTgDCX
5 µm
E
WT
200 nm
F
ΔTgDCX
G
ΔTgDCX/TgDCX
H
ΔTgDCX/
TgDCX71-243
I
WT
1 cm
ΔTgDCX
ΔTgDCX/TgDCX
ΔTgDCX/TgDCX71-243

Figure 5

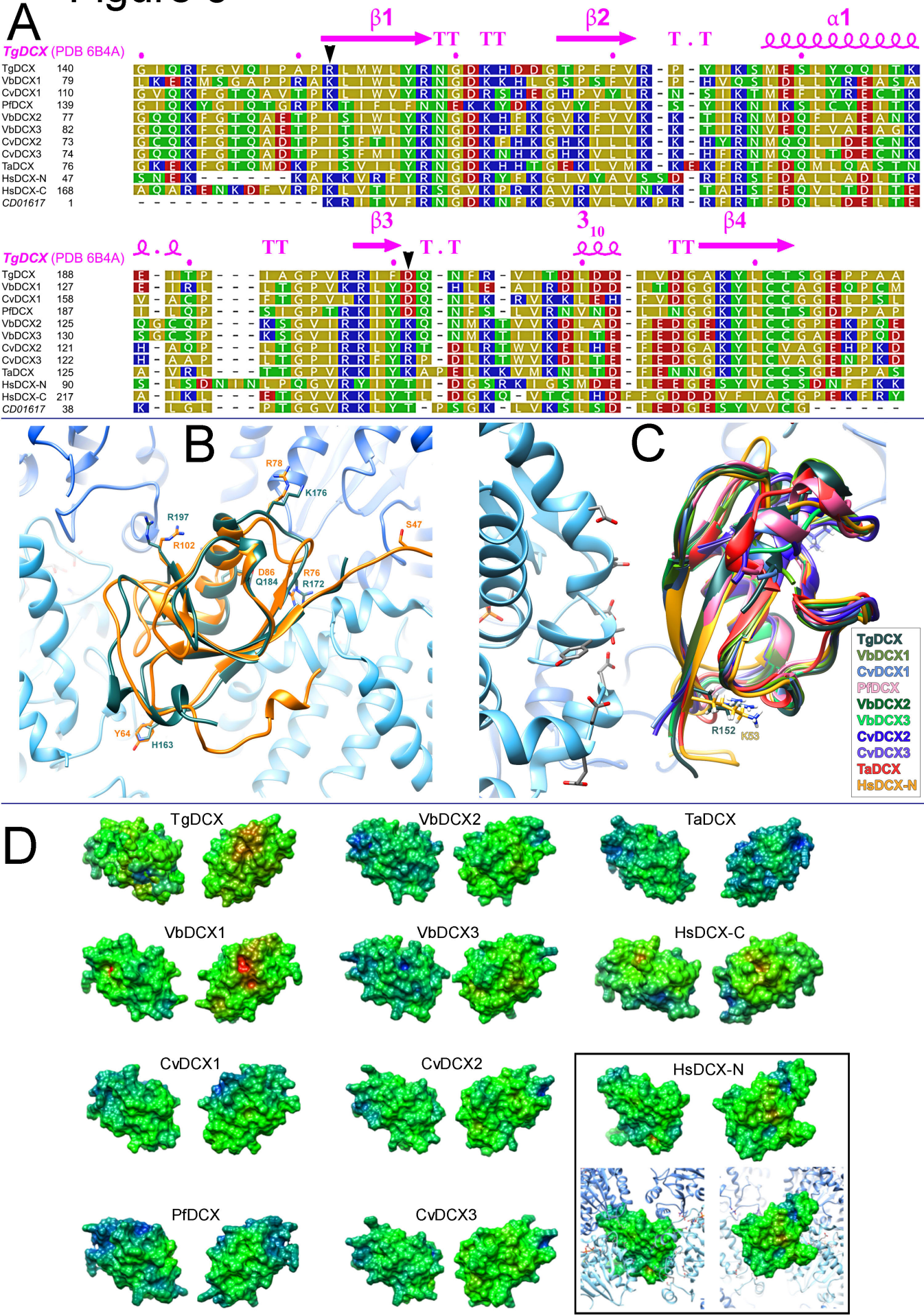
A
TgDCX (PDB 6B4A)
β1
TT
TT
β2
T . T
α1
TgDCX 140
VbDCX1 79
CvDCX1 110
PfDCX 139
VbDCX2 77
VbDCX3 82
CvDCX2 73
CvDCX3 74
TaDCX 76
HsDCX-N 47
HsDCX-C 168
CD01617 1
β3
TT
T . T
3 10
TT
β4
TgDCX (PDB 6B4A)
TgDCX 188
VbDCX1 127
CvDCX1 158
PfDCX 187
VbDCX2 125
VbDCX3 130
CvDCX2 121
CvDCX3 122
TaDCX 125
HsDCX-N 90
HsDCX-C 217
CD01617 38
B
R78
K176
R197
R102
S47
D86
Q184
R76
R172
Y64
H163
C
R152
K53
TgDCX
VbDCX1
CvDCX1
PfDCX
VbDCX2
VbDCX3
CvDCX2
CvDCX3
TaDCX
HsDCX-N
D
TgDCX
VbDCX2
TaDCX
VbDCX1
VbDCX3
HsDCX-C
CvDCX1
CvDCX2
HsDCX-N
PfDCX
CvDCX3

Figure 6

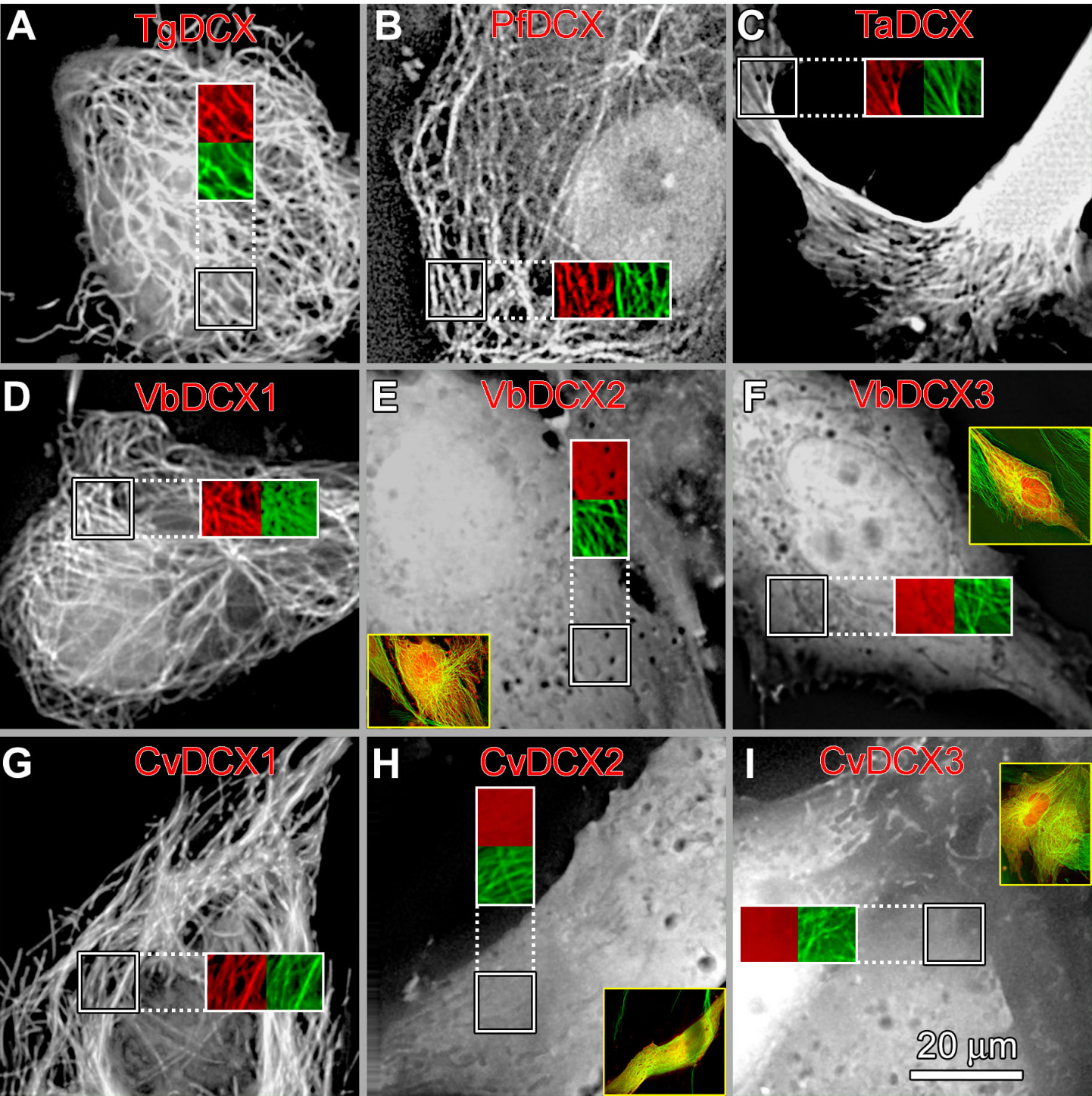
A
TgDCX
B
PfDCX
C
TaDCX
D
VbDCX1
E
VbDCX2
F
VbDCX3
G
CvDCX1
H
CvDCX2
I
CvDCX3
20 µm

Figure 7

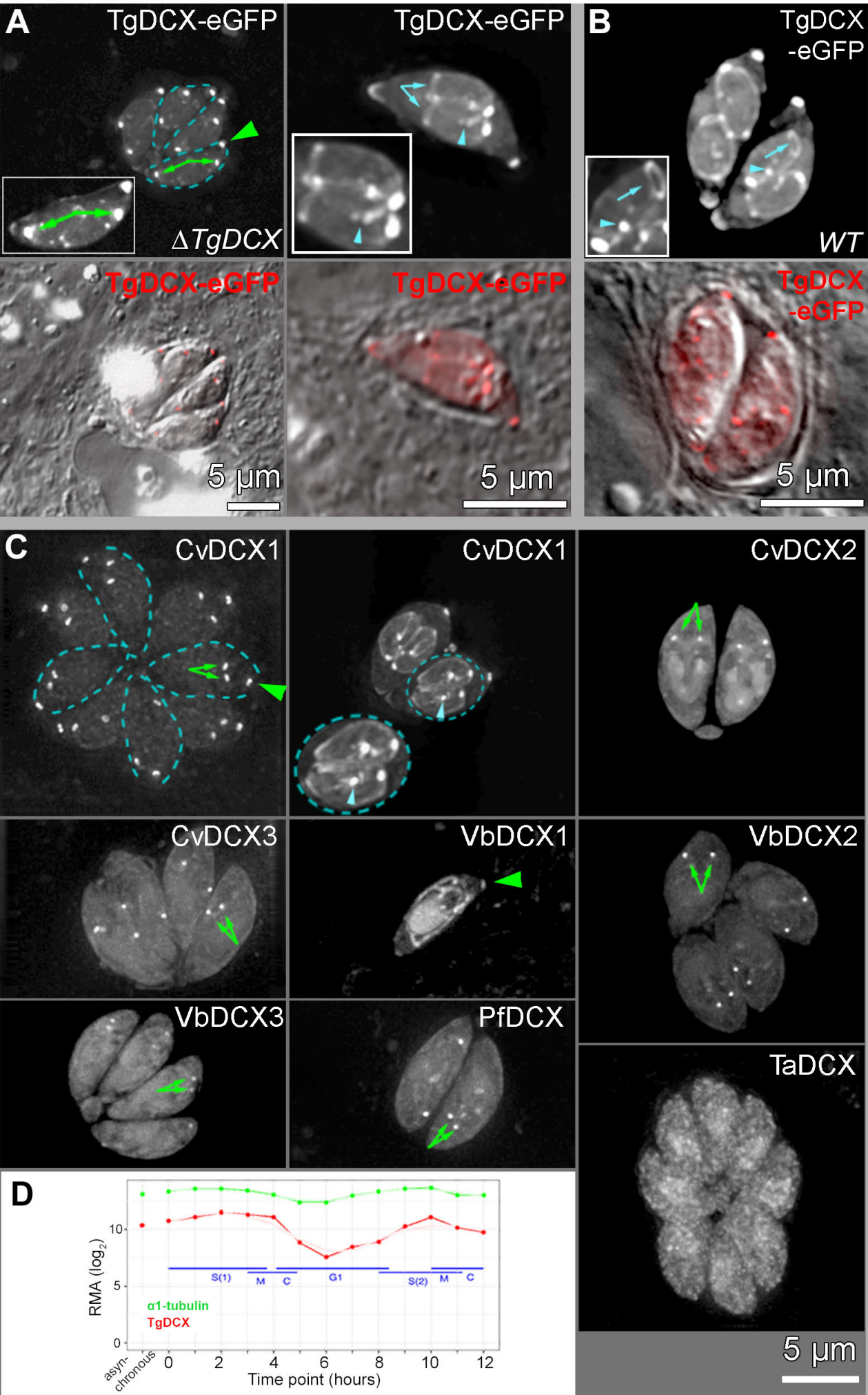
A
TgDCX-eGFP
ΔTgDCX
TgDCX-eGFP
B
TgDCX
-eGFP
WT
TgDCX-eGFP
5 µm
TgDCX-eGFP
5 µm
TgDCX
-eGFP
5 µm
C
CvDCX1
CvDCX1
CvDCX2
CvDCX3
VbDCX1
VbDCX2
VbDCX3
PfDCX
TaDCX
5 µm
D
RMA (log2)
10
5
0
S(1)
M
C
G1
S(2)
M
C
α1-tubulin
TgDCX
asyn-
chronous
0
2
4
6
8
10
12
Time point (hours)

Figure 8

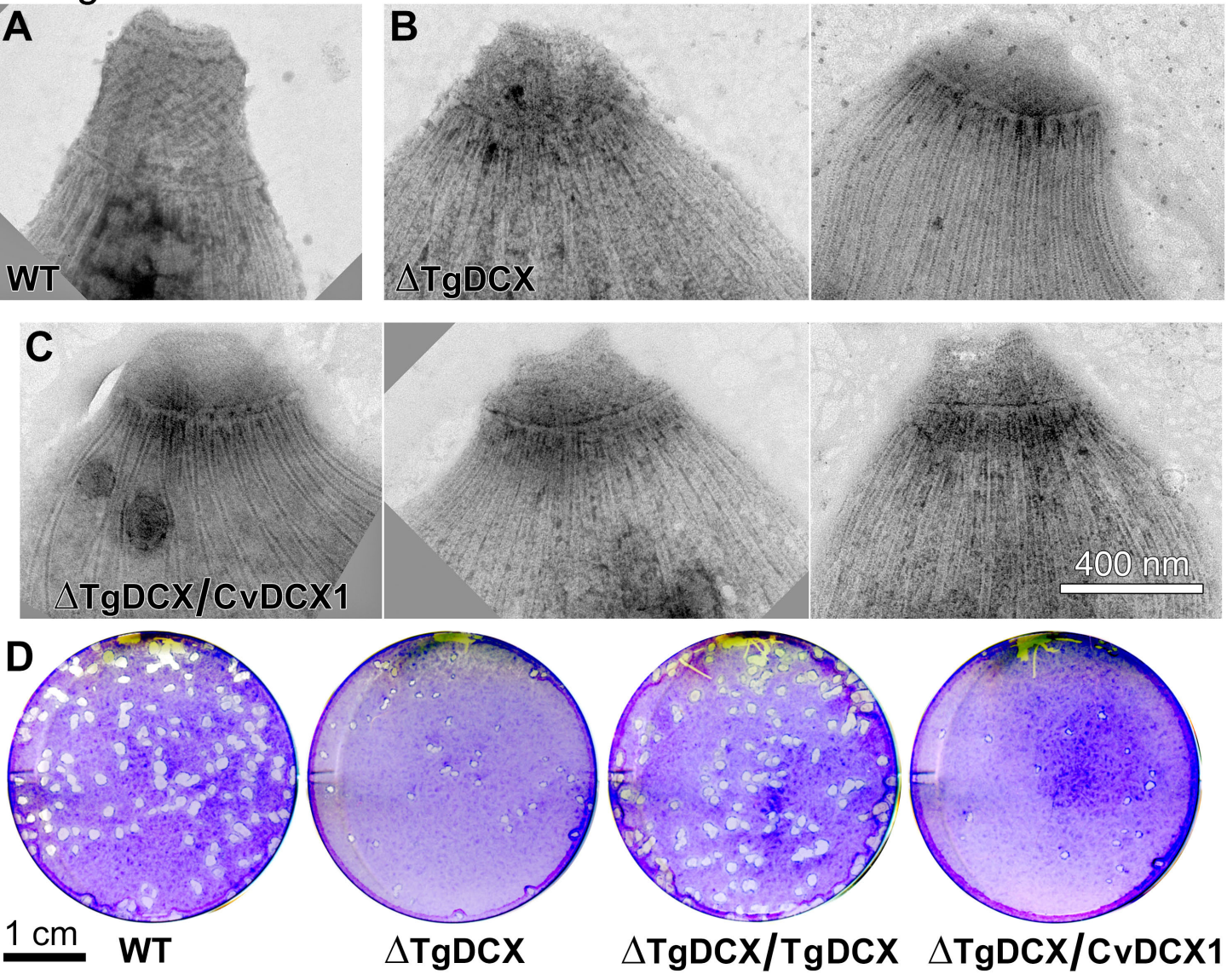
A
WT
B
ΔTgDCX
C
ΔTgDCX/CvDCX1
400 nm
D
1 cm
WT
ΔTgDCX
ΔTgDCX/TgDCX
ΔTgDCX/CvDCX1

Figure 9

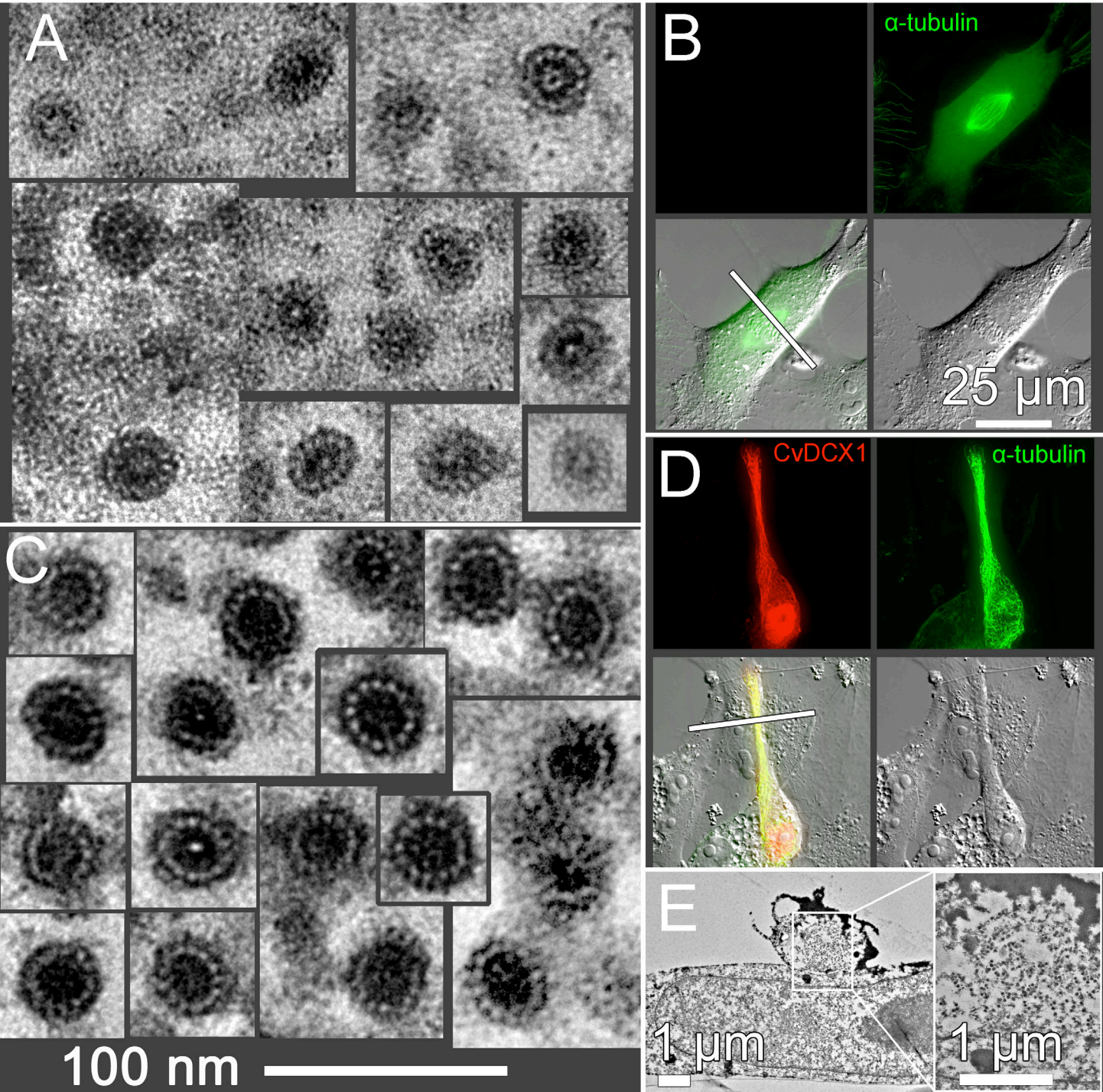

Figure 10

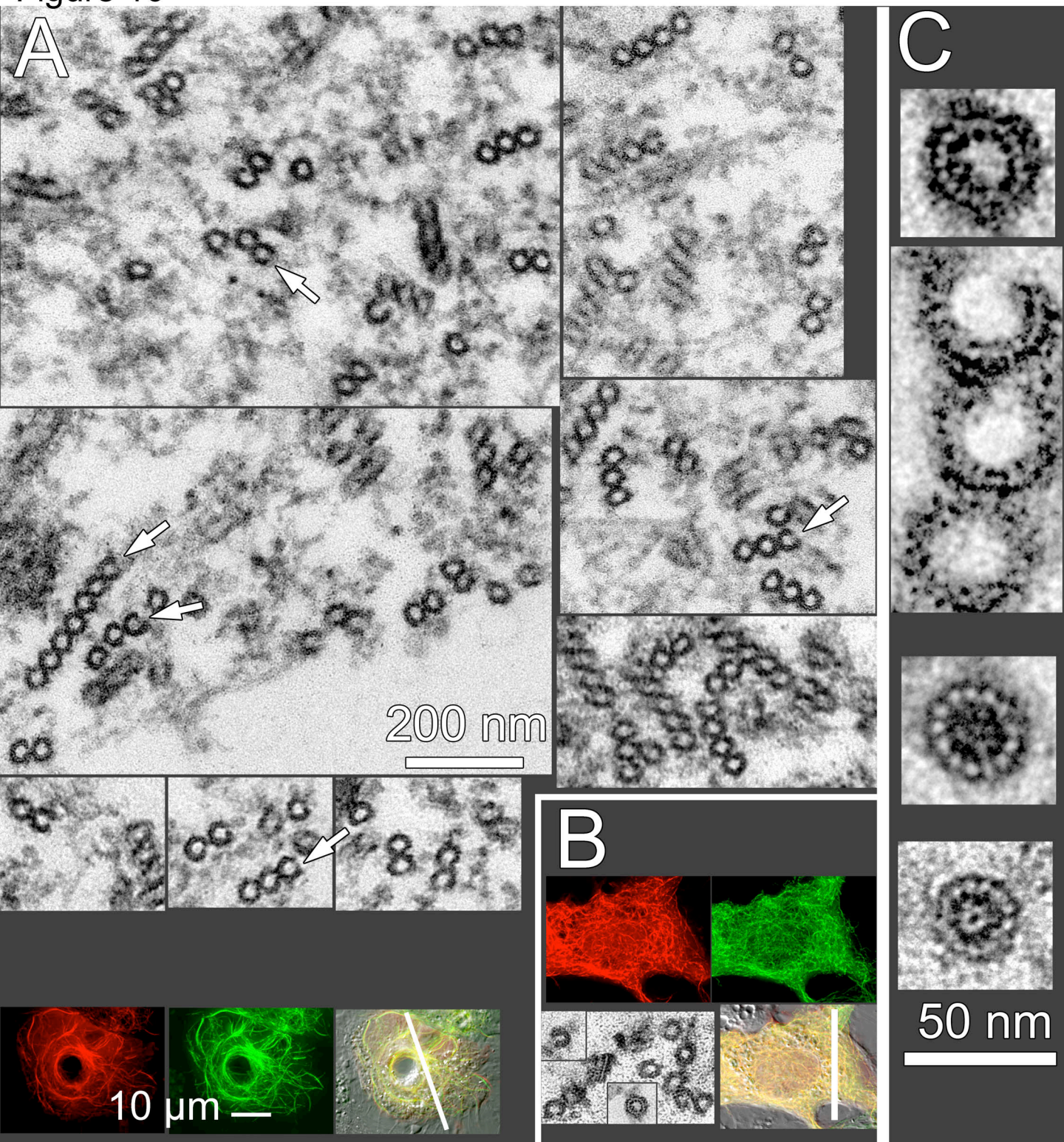
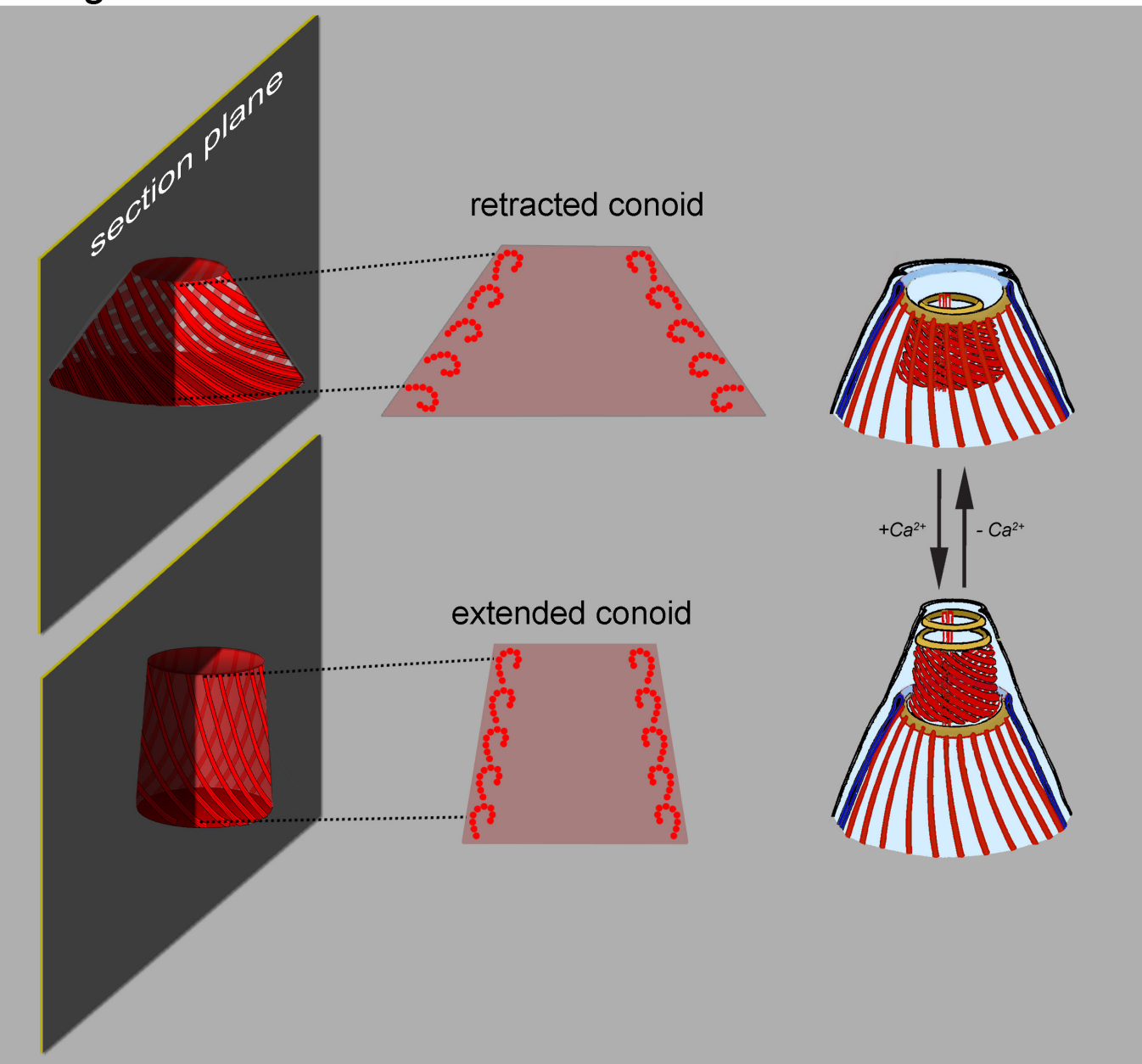
Figure 11